FACULDADE DE ENGENHARIA DA UNIVERSIDADE DO PORTO

CMOS Design for Indoor Photovoltaic Harvesting

Ana Luísa Cardoso Macedo

Mestrado Integrado em Engenharia Eletrotécnica e de Computadores

Supervisor: Cândido Duarte

October 12, 2021

Abstract

The present work aims to study a photovoltaic (PV) energy conversion system for indoor applications. This system consists of a PV cell, a DC-DC switched capacitor (SC) and an energy storage element. It is common to PV harvesting systems to use maximum power point tracking (MPPT) methods in order to extract the maximum power from the PV cell. However, these methods do not guarantee the maximum power is delivered to the load, being lost in the DC-DC SC.

It is important to also guarantee the maximum power point is transferred. Thus, this system aims to guarantee the maximum power is being harvested but also the maximum power is being storage to the storage element.

The power conditioning stage consist of a cross coupled voltage doubler charge pump and a undervoltage lockout circuit between the PV cell and the switched capacitor. This stage guarantees the charge pump only operates when the energy available is sufficient for its correct operation. The output connects to a supercapactior where the energy is stored. Several simulations were made to analyse the performance of the system.

Resumo

O presente trabalho estuda um sistema de conversão de energia fotovoltaica para aplicações em ambientes interiores. O sistema é composto por uma célula fotovoltaica, um conversor de corrente contínua para corrente contínua de capacidades comutadas e um elemento de armazenamento de energia.

É frequente que um sistema de recolha de energia fotovoltaica se baseie num método que permita que a máxima potência seja extraída da célula. Porém esses métodos não garantem que a máxima potência seja entregue à carga, perdendo-se no conversor. É igualmente importante garantir que se transfere a máxima potência. Assim, o sistema proposto visa não só garantir que a máxima potência é recolhida, mas também que a máxima potência é guardada no dispositivo de armazenamento.

O nível de condicionamento de energia é composto por um *charge pump* duplicador de tensão e um circuito de arranque entre a célula fotovoltaica e o conversor. Garantindo assim que o *charge pump* apenas opera quando a energia disponível é suficiente para o seu correto funcionamento. A saída é ligada a um super condensador, onde é armazenada energia. Foram feitas diversas simulações para estudar a performance do sistema.

Agradecimentos

Em primeiro lugar, terei de agradecer aos meus pais, à minha irmã e ao Miguel. Sei que nunca terei agradecimentos suficientes por todo apoio e carinho que recebi não só enquanto realizei esta dissertação, mas por todos os outros momentos em que nunca deixaram de acreditar em mim.

Ao meu orientador, ao Professor Cândido Duarte, por todas horas dispensadas, pela partilha incansável de conhecimento e pelo apoio que me deu para a concretização desta dissertação.

A todos os amigos que fiz ao longo deste percurso pela FEUP, por toda a companhia nas horas de alegria e festa e nas horas de desespero antes de cada exame ou entrega. Sei que sem vocês estes anos não teriam sido metade do que foram.

À minha restante família, em especial à minha avó Beatriz, que mesmo longe nunca deixou de estar presente, e às minhas queridas Cardosas, inesgotáveis nos abraços e acima de tudo pelo exemplo diário que são para mim.

Não poderei deixar de agradecer aos amigos de infância que se tornaram amigos da idade adulta também, por nunca se esquecerem da sua amiga ausente que para pouco pela terrinha.

E por último, à minha Luisinha, que não pode ver o final desta etapa, mas que teve um dos papeis mais importantes nos primeiros vinte anos da minha vida. A sua força de carácter, levarei comigo todos os dias.

"Say goodbye to all the times you felt lost,
to all the times it was a No instead of a Yes,
to all the scrapes and bruises, to all the heartache."

Lily Aldrin

Contents

List of Figures

List of Tables

Acronyms and Abbreviations

ANN	Artificial Neural Network
C_{Load}	Load Capacitance
CMOS	Complementary Metal Oxide Semiconductor
EPP	Estimated-Perturb-Perturb
FL	Fuzzy Logic
FOCV	Fractional Open-Circuit Voltage
FSCI	Fractional Short-Circuit Current
HP	High-Pass
Inc-Cond	Incremental Conductance
I_{OUT}	Output Current
LDO	Low Dropout Regulator
Li-Ion	Lithium Ion
LP	Low-Pass
MOS	Metal-Oxide Semiconductor
MPP	Maximum Power Point
MPPT	Maximum Power Point Tracking
NiCd	Nickel Cadmium
NiMH	Nickel Metal Hydride
NMOS	N-Channel Metal Oxide Semiconductor
OCC	One-Cycle Control
$P_{INsource}$	Input Power on the source
$P_{INsupply}$	Input Power on the supply
PMOS	P-Channel Metal Oxide Semiconductor
P_{OUT}	Output Power
PSS	Periodic Steady-State Analysis
PV	Photovoltaic
PWM	Pulse with Modulation
RCC	Ripple Correlation Control
SC	Switched Capacitor
SLA	Sealed Lead Acidd
SMB	Sliding-Mode-Based
ULC	Undervoltage Lockout Circuit
V	Volt
V_{IN}	Input Voltage
V_{OUT}	Output Voltage
V_{REF}	Reference Voltage

Chapter 1

Introduction

1.1 Motivation

Nowadays, energy production is one of the biggest concerns of environmentalists due to the high levels of pollution produced. Greenhouse gases make the planet warmer everyday. This temperature increase is mainly attributed to actions of humans. More than a quarter of greenhouse emissions arise from the burning of fossil fuel, heat and transportation, which is directly connected with electricity generation, transmission and distribution. The vast majority of these gas emissions are from carbon dioxide, released during the combustion of fossil fuels, such as coal, natural gas and oil, all used in electricity production.

More sustainable energy sources are therefore becoming a subject of paramount importance, and renewable energies are manifestly the more sustainable ones. There are several natural resources from which energy can be extracted. Several studies have been reinforcing that solar energy is the renewable energy with the biggest energy exploitation — however, improvements are required in order to increase its viability as the predominant energy source in the market. The ability to harvest energy when there is no solar exposure or when it is significantly reduced — as is the case in indoor environments — is the primary focus of this dissertation.

Integrated circuits, namely those that make use of Complementary Metal–Oxide–Semiconductor (CMOS) technology, are getting smaller over time. The portability of these components is becoming more significant. The way such components are being supplied is, therefore, getting more attention in the scientific research. Any electronic device exposed to environmental conditions can harvest energy for its own use. Although it is very difficult for a device to be exclusively powered by harvested energy (from sunlight or artificial light), being able to increase its battery lifetime is crucial, and any energy contribution can be valuable.

Light energy harvesting depends on the ambient light available, which can be natural, solar light, or an artificial form, like a light bulb. In this thesis the main focus will be on energy harvesting from artificial light.

1.2 Goals

This thesis proposes the study, design and implementation of PV energy harvesting system. The proposed design aims to maximize the power transfer from the PV cell, adjusting the circuit parameters to this specific target.

This system, as other state-of-art system [1], is mainly composed of a PV cell, a step-up DC-DC converter —Charge Pump— and an energy buffer, where energy will be stored, figure 1.1. Some other components, like rectifiers, phase controllers, Low Dropout Regulators or Start Ups, may also be needed [2–6]. The system proposed in [7] is simpler, it is a batteryless ultralow-power energy supply system, composed of an organic PV cell and a CMOS PMU.

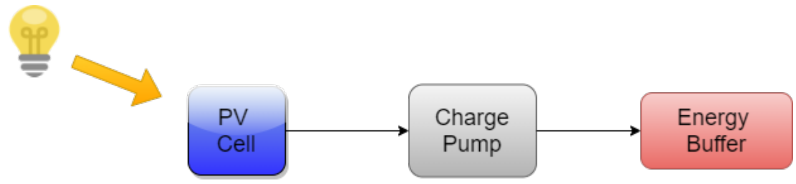

Figure 1.1: Proposed System.

The main goal of this project is to find the most adequate topology for this system and design it in a CMOS process. All the designs were created using Cadence Virtuoso Analog Design Environment and validated in simulation.

1.3 Structure of the Document

This document is structured in five chapters. Chapter 1 is an introductory chapter. Chapter 2 is the current state of art of PV energy harvesting systems, charge pumps models, supercapacitors and Maximum Power Point Tracking (MPPT) methods. In Chapter 3, it is presented the methodology for the most crucial stage of the PV system, the Power Conditioning Stage, and the test benches implemented to evaluate this stage as well as the results of the several simulations performed. In Chapter 4 it is presented a final model for the PV system, including a PV cell, the test bench used and the results of the tests performed are also introduced in this chapter. Finally, Chapter 5 is a conclusions chapter, were it is presented the final remarks of this dissertation and future work.

Chapter 2

Fundamentals of Photovoltaic Harvesting

This chapter presents the fundamental aspects related with photovoltaic cells as energy supply modules and associated design of CMOS circuits. Typical components of such circuits are presented, as well as their main purpose and issues most commonly found when trying to apply/use them.

2.1 Photovoltaic Cells

A PV system is responsible for the direct conversion of sunlight into electricity. Nowadays, the vast majority of PV devices use a single junction to create an electric field within a semiconductor, like a PV cell. A PV cell is a semiconductor diode whose p-n junction is exposed to light [8], where the cells can be organized either in panels or in arrays [1, 9]. Furthermore, the PV panels can be connected in series or in parallel to form large PV systems, improving voltage or current output.

There are several types of semiconductor materials used in PV cells. Silicon (Si) is the most common material used in the manufacturing of PV cells, representing approximately 90% of market sales, mostly due to its abundance in our planet. Silicon is also the most common semiconductor on computer chips, and as such, it is a tried and tested technology. The composition of PV cells is either based on a thin layer of bulk Si or a thin Si film attached to electric terminals. One of the sides of this layer will form the p-n junction [9]. The basic anatomy of a Si PV cell can be observed in Figure 2.1. Particularly noteworthy is the metal grid on the side of the semiconductor, which is exposed to the light. The most common Si cells are either monocrystalline or polycrystalline.

Each monocrystalline cell is a single crystal of Si. The silicon is formed into bars and then cut into wafers. By using a single Silicon crystal, the amount of impurities can be minimized. Monocrystalline PV cells have several advantages, such as their high purity, due to the presence of a single crystal and their efficiency when compared to other PV cells. However, the process

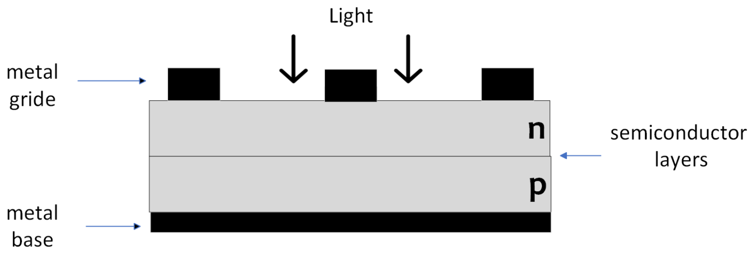

Figure 2.1: Physical structure of a PV Cell. Adapted from [9].

involved in the manufacturing of monocrystalline PV cells is significantly complex and as such, they tend towards a higher price relative to their alternatives.

Polycrystalline PV cells, in opositon to monocrystalline ones, are made by melting various Si fragments so the wafers, that are later incorporated in the PV panel, can be formed. The aforementioned process is less complex than the one required to produce monocrystalline Si cells, which means that these can be found at a lower price. Polycrystalline cells can also be referred as multi-crystalline or many-crystal cells. Since there are many crystals per cell, the electrons have less space to move through the cell, which results in less efficiency when compared to monocrystalline cells. As regards to the aspect, pollycristalline solar panels have a blue tone and the monocrystalline a black tone. Nowadays, monocrystalline solar panels are the most popular.

When the incidence of light in the cell occurs, if the cell is short circuited, electric current will be generated. The light is absorbed, charge carriers are created in the p-n junction, and later these carriers will be collected at the terminals of the PV system. The rate at which the carriers are generated depends on the flux of incident light as well as on the absorption characteristics of the semiconductor of the PV cell. Regarding the power we can extract from the PV cell, as stated in [10] *"Maximum power is delivered to the load when its impedance matches that of illuminated device"*.

The ideal model of a PV cell can be described as:

$$I = I_{pv} - I_{0,cell}[e^{\frac{qV}{AkT}} - 1] \tag{2.1}$$

where $I_{pv,cell}$ is the incident light current, which is proportional to the sun irradiation, $I_{0,cell}$ is the reverse saturation or leakage current of the diode, q is the electron charge (1.60x10^{-19} C), k is the Boltzmann constant (1.38x10^{-23}J/K), T is the temperature, in Kelvin, of the p-n junction and A is the diode ideality constant.

The authors in [7] use an organic PV cell on their proposed harvesting system instead of a silicon-semiconductor. These organic PV cells are based on heterojunctions of organic semiconductors, such as organic compounds, polymers or carbon-nanoparticles. These compounds are soluble in ordinary solvents which makes it possible for the organic layer to be processed from solutions [7]. Organic PV cells are lightweight and flexible, and their performance under diffuse light makes them more suitable for use in applications that more common technologies, such as silicon PV cells, do not accommodate to.

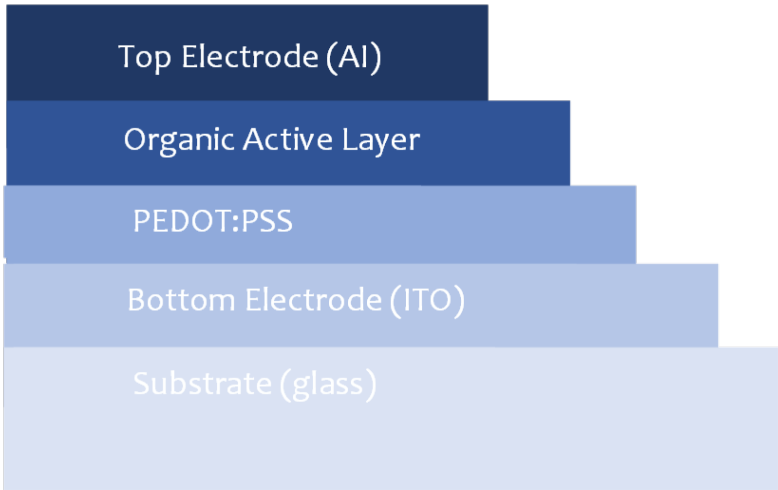

Figure 2.2: Structure of the OPV cell used in [7]. Adapted from [7].

2.2 Energy Conditioning

The energy harvested from the PV cells is not enough to supply complex applications, such as wireless microsensors [1]. Thus, in most cases, the need arises for a DC-DC converter to process the electricity from the PV system and boost it.

One of the biggest challenges in the field of circuitry is to find the best way to convert a DC source into a lower or higher voltage. For AC voltages, a transformer can be employed, however the same does not apply to DC voltages. A possible solution would be to divide the low DC voltage by employing an oscillator, passing the resulting AC waveform through a step up transformer and filtering it. The problem with this approach lies in the need for a transformer, an inductive component, which is relatively larger and has a higher cost than most components. So, circuit designers came up with other topologies.

2.2.1 Charge Pump

A charge pump uses a capacitor to store higher voltages. Its operation is quite simple. It works like a switching regulator, providing energy by charging and discharging elements. In theory, diodes can be used for current flow control. However, in practical applications, switches are replaced with MOSFETs and the capacitors are external devices, that can be ceramic or electrolytic depending on how much capacitance is needed.

The clear advantage of a charge pump is the fact that an inductor is not needed, resulting in a smaller circuit size. It is more efficient than linear regulators, its design is relatively simple, and the costs are low. Therefore, we will focus on charge pumps that do not have an inductor on their structure, more commonly known as Switched Capacitors (SC). They are also very popular due to their accurate discrete-time frequency responses, good linearity and dynamic range. Using a SC, it is possible to get significantly higher levels of accuracy when compared to integrated RC circuits.

A SC is built like every charge pump, with a capacitor and switches, op amps and non overlapping clocks. Switched capacitors are divided in several topologies:

- *Dickson Charge Pump*: The first charge pump was proposed by John F. Dickson [11] in 1976. The circuit is represented in Figure 2.3. In this Charge Pump the coupling capacitors are connected in parallel through a diode. This way the charge pump is able to function efficiently even with high bottom plate parasitic capacitance [12].

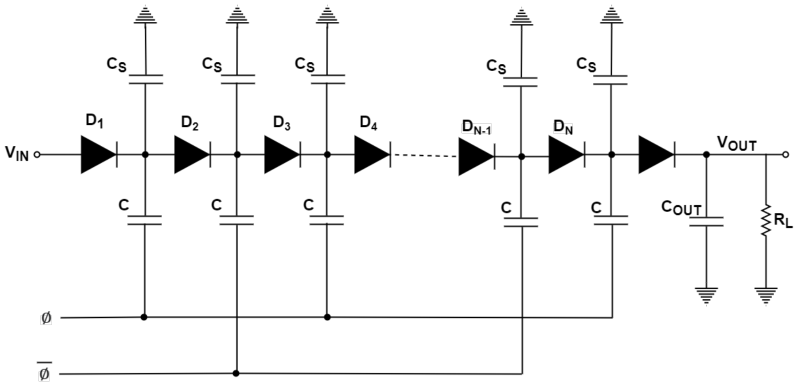

Figure 2.3: Dickson Charge Pump Circuit. Adapted from [12].

Another positive aspect of this SC lies in the fact that the drive capability operates well even with a higher number of multiplier stages.

On the other hand, the first Dickson charge pump uses diodes, instead of switches, as the charger transfer device. This leads to an output reduction and consequently the efficiency of the converter is also reduced. Thus, researchers came up with new versions of the Dickson charge pump, capable of overcoming the issues of the original one. The rest of the switched capacitors covered in the section use either the Dickson topology or a modified version of it.

- *The Bootstrap Charge Pump*: This converter uses Metal-Oxide Semiconductor (MOS) transistors as switches instead of diodes. These transistors have to be switched ON by applying

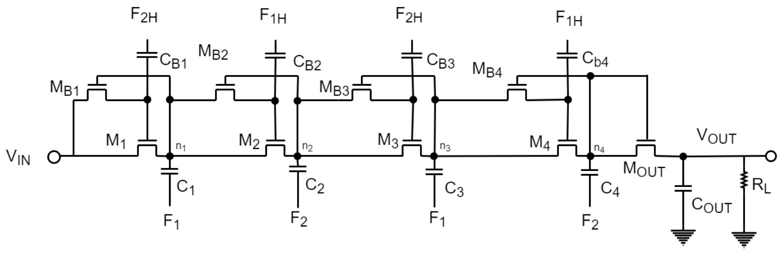

Figure 2.4: Schematic Diagram of a Bootstrap Charge Pump. Adapted from [12].

gate voltages higher than their source terminal voltages. This needs to be done because in a charge pump the voltage at the switch terminals is higher than their source terminal voltages [13].

Figure 2.4 presents the power stage of a Bootstrap charge pump with four stages. Each stage is composed of one pass transistor (M_{1-4}), one pumping capacitor (C), one supporting transistor (M_{B1-4}) and one supporting capacitor (C_b). During the first half period F_1 and F_{1H} are high, and F_2 and F_{2H} are low. The gate of transistors, M_1, M_3 and M_{OUT} are charged to their drain voltage by M_{B1} and M_{B3}, and operates like reverse bias diodes, due to their source voltage being higher than their gate and drain voltages. When M_{B2} and M_{B4} are off, M_2 and M_4 turn ON and their gate voltages is $2V_{IN}$ higher than their drain voltage. Consequently, charge passes from n_1 to n_2 and from n_3 to n_4. During the next half period, the opposite happens, since F_1 and F_{1H} are low, and F_2 and F_{2H} are high. Charge is transferred from V_{IN} to n_1 and from n_2 to n_4. [12]

The downside of this step-up converter is that it requires four phase clocks and a double voltage swing in some of the clock signals. Nevertheless, higher efficiency and higher output voltage compensate its limitation.

- *Fibonacci Charge Pump*: The Fibonacci Charge Pump presents the highest gain to capacitor number ratio. Thus, it is very popular when a higher conversion gain is necessary. This step-up converter is composed only by three capacitors and ten switches and operates with a two-phase clock, as can be seen in Figure 2.5. Each transfer capacitor (C_{1-3}) is charged to the voltage of the previous stage boosted, and then it increases the voltage of the following stage [12, 14]. The ideal voltage gain of a Fibonacci charge pump is $G = F_{N+1}$, where N is the number of stages and F_N is the N-th Fibonacci number.

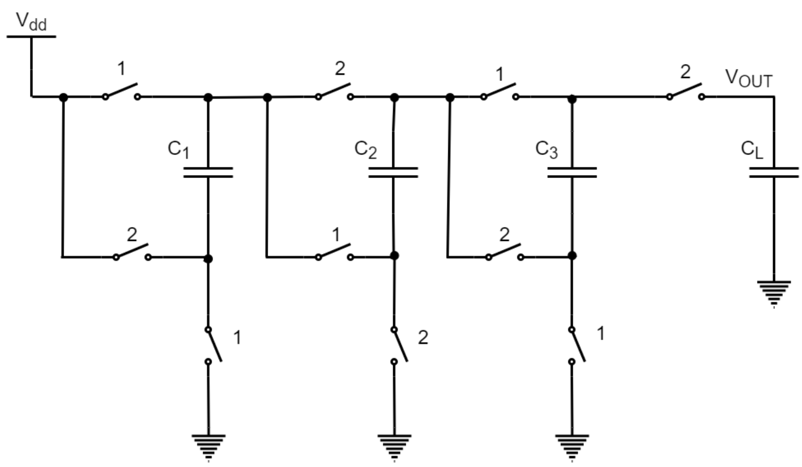

Figure 2.5: Schematic diagram of a 3-stage Fibonacci Charge Pump (N = 3, G=5). Adapted from [14].

- *Series-Parallel Charge Pump*: This type of charge pump is characterised by the following method of operation: during the first half period, when switches $P_{1,2}$ and $P'_{1,2}$ are closed and switches, S_{1-3}, are open, the capacitors charge the power supply, V_{DD}, in parallel, and during the rest of the period, when switches $P_{1,2}$ and $P'_{1,2}$ are open and switches, S_{1-3}, are closed, the capacitors are connected in series, as can be seen in Figure 2.6. The principal limitation of this topology is the presence of parasitic capacitances, which has a negative impact on the behaviour and performance of the converter. The lower output voltage, when comparing with an ideal charge pump, with no parasitic capacitances, allows for a higher number of stages [13].

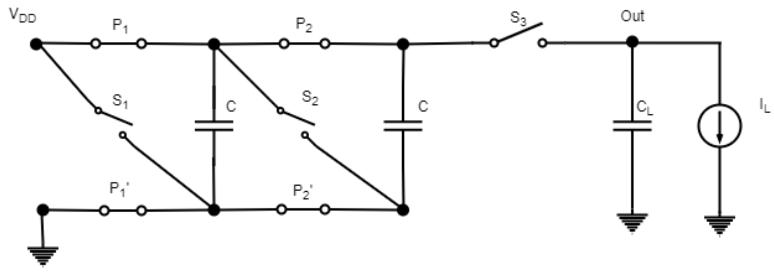

Figure 2.6: Series-parallel Charge Pump. Adapted from [13].

- *Voltage Doubler*: The voltage doubler is the most common topology. In this converter, two cells of voltage doubler operate in parallel with a different phase, as can be seen in Figure 2.7. In every half period the pumping capacitor charges the output which reduces the output voltage ripple by half. Gate drive circuit becomes unnecessary since the gates of the power transistors are operated by the internal node of the power stage [12].

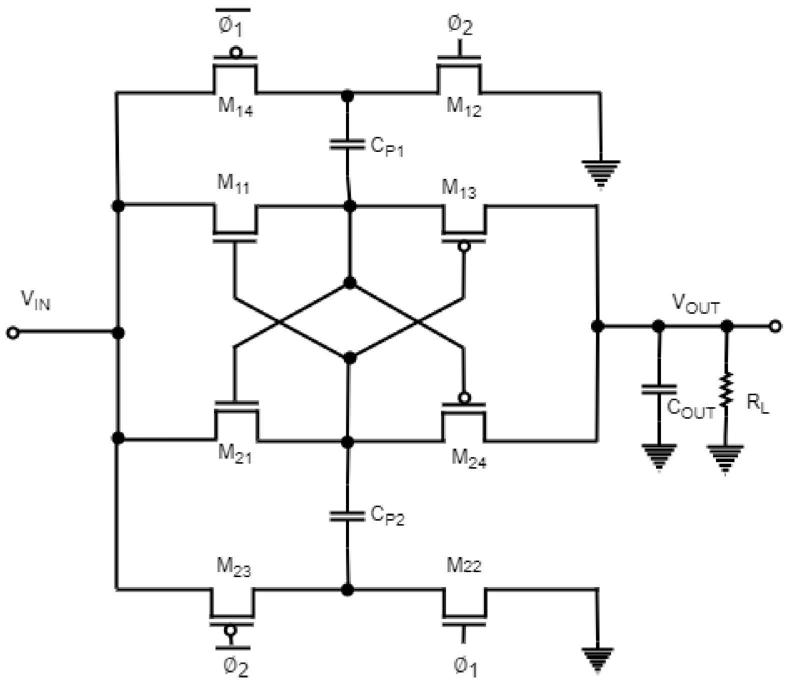

Figure 2.7: Cross-coupled Voltage Doubler. Adapted from [12].

It would be easier to understand a switched-capacitor circuit if ideal op-amps were assumed. However a real-life scenario should be considered where op-amps are non-ideal in a number of areas, such as DC gain, unity-gain frequency, phase-margin, slew rate, and DC offset since all these nonidealities impact the circuit performance.

The authors in [15] proposed a closed-loop scheme of high-gain serial-parallel switched-capacitor step-up converter. This approach combines a phase generator and a pulse-width-modulation (PWM) controller for step-up DC-DC conversion and regulation. The circuit configuration of the proposed SC step-up converter was divided in two parts, namely the power part and the control part. The power stage was composed of two three-stage SC cells, each cell with three pumping capacitors in cascade between the source and the output. These capacitors were charged in parallel and discharged in series. This allowed for a higher voltage gain, since each cell could be considered a step-up converter with four times the voltage gain. The control stage consisted of a low-pass filter, a PWM block, and a phase generator.

Another approach in [16] presented a single switch step-up converter derived from a flyback converter. The first proposed single switch step-up converter modifies the regular configuration of a flyback converter by adopting a voltage doubler rectifier. This allows for an easing of the voltage stress on the diode, which is a problem associated with these converters. To reduce the stresses on the switch and diodes even more, the authors presented a new non-isolated single Switch high step-up converter, adding an additional capacitor and reorganizing the components.

Although we are more interested in a DC-DC converter able to step up power for this system, when the ratio between the input voltage and the output voltage is low, Low Dropout Regulators (LDOs) are more effective. As such, the role of LDOs on PV Systems should also be covered.

2.2.2 Low Dropouts Regulators

A LDO is a linear voltage regulator conceived to maintain regulation with very low dropout voltage, the voltage difference between the output voltage and the input voltage, so the power dissipated as heat on the device is minimal and thus the conversion efficiency can be increased. They usually consist of a series pass transistor, a reference voltage and a feedback amplifier that controls the voltage drop of the transistor. Unlike charge pumps, LDOs do not generate ripple and thus it is possible to get a very clean supply voltage. Its design is very simple, since the number of external passive components needed is very low, and thus, it is an inexpensive method. Figure 2.8 shows an example of a LDO implementation using a Capacitor P-Channel Metal-Oxide Semiconductor (PMOS). They are very useful for any hardware that requires a constant and stable voltage while minimizing the upstream voltage.

For example, in PV systems like the one in [18], the LDO is used to generate internal bandgap-stabilized supply voltage and the bias currents for the functional blocks. The PV system implemented by the authors in [19] makes use of a LDO to maintain a stable output of 1V, the adequate value for sensor wireless networks, the type of network the proposed indoor PV energy harvesting

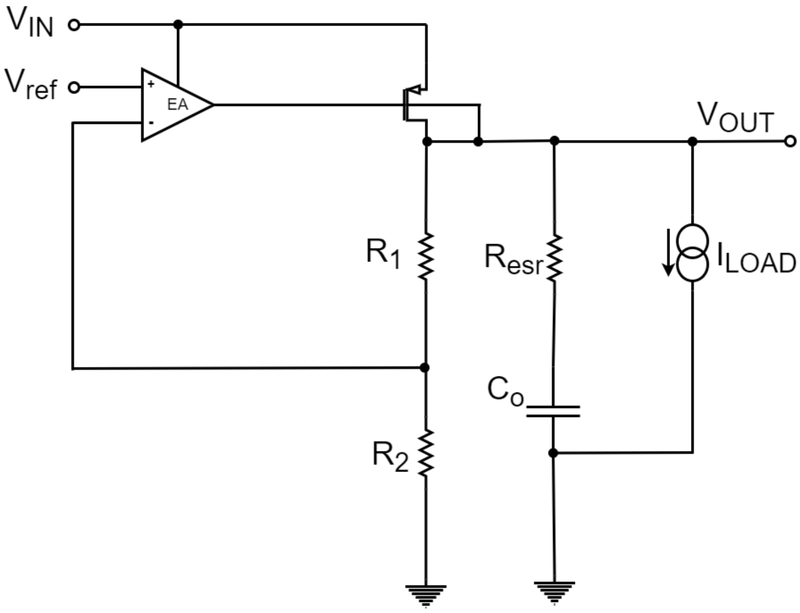

Figure 2.8: External Capacitor PMOS LDO. Adapted from [17].

system supplies.

2.3 Energy Storage

As said in section 1.2 an energy buffer is one of the components of the system this thesis proposes. The storage technology chosen will play a crucial role in harvesting systems. Rechargeable batteries are a popular choice for energy storage in microsystems applications. Based on their chemical composition we can list several technologies: Sealed Lead Acid (SLA), Nickel Cadmium (NiCd), Nickel Metal Hydride (NiMH) and Lithium Ion (Li-ion). It is possible to characterize the different battery technologies considering their energy density, power density, charge-discharge efficiency, self discharge rate and number of deep recharge cycles [20].

When choosing the battery technology it is important to take into account the memory effect, the loss of energy capacity due to repeated *shallow recharge*, which consists of recharging a partial discharged battery, and the battery charging process. The charging process, as required in Lithium batteries, can be *pulse charging*, which means that relaxation periods and discharge pulses are applied during the charging process, these periods are able to eliminate concentration polarization and increase the power transfer rate, and consequently the charging process becomes faster [21]. It is used a high pulsating current to charge the battery. Commonly is needed an auxiliary battery or a charging circuit in this case, representing additional complexity to the system. NiMH batteries can be *trickle charged*, its operation is quite simple, it is just needed to apply an energy source directly to the terminals [20]. When using trickle charging, the battery is charged slowly, over a period of time. This way there is no need to recharge the battery periodically, since it is being charged all the time with a smaller amount, thus there is no risk of overcharging.

Battery Type	Normal Voltage (V)	Capacity (mAh)	Weight Energy Density (Wh/kg)	Power Density (W/kg)	Efficiency (%)	Self Discharge (%/month)	Charging Method	Recharge Cycles
SLA	6	1,300	26	180	70-92	20	Trickle	500-800
NiCd	1.2	1,100	42	150	70-90	10	Trickle	1,500
NiMH	1.2	2,500	100	250-1,000	66	20	Trickle	1,000
Li-ion	3.7	740	165	1,800	99.9	<10	Pulse	1,200
Li-polymer	3.7	930	156	3,000	99.8	<10	Pulse	500-1,000

Table 2.1: Comparison of Rechargeable Battery Technologies [20]

Even though batteries have a low cost and are wide available, they may not be the best option for PV Energy Systems because PV cells are not an ideal source of energy to charge a battery. Alternatively to rechargeable batteries we can use a supercapacitor.

Supercapactiors or electrolytic double layer capacitors are one of the most adequate energy storage components for the system proposed since: they have a longer life when compared to ordinary batteries, they have high power rating, there is no limitation on deep cycle use and the impact of supercapacitors on the environment is very low [22]. Additionally supercapacitors do not suffer from memory effect and are trickle charged [20]. Applying a voltage to the supercapacitor terminals forms a double layer at the junction of the electrode and the electrolyte [23].

A supercapacitor distinguishes itself from a regular capacitor on two important aspects: The area of the plates, on a supercapacitor, is larger and there is less distance between the plates. This is explained due to the fact that the interface between the plates is quite different in a supercapacitor. On a common capacitor this interface is a thick dielectric, which is made of mica and a thin plastic layer or simply air. The other difference relates to how the plates deal with charge. Once a capacitor is charged, one of the plates will be positively charged and the other one negatively charged, creating an electric field between them. Whereas, in a supercapacitor there is no dielectric. Instead both plates are soaked in an electrolyte and separated with a very thin insulator, it can be coal, paper or plastic. Once the plates are charged an opposite charge is formed on the other side of the separator, creating a double electric layer. Furthermore the cycle efficiency of a supercapacitor is close to 100%.

2.4 Maximum Power Point Tracking

We can denote two major problems with PV systems, namely the conversion efficiency of PV cells, and the constant weather changes that impact the power generated on the PV system. The efficiency can be improved by using a MPPT Method. These methods are used to extract the maximum power from a PV system and then transferred it to the load [24, 25]. The Maximum Power Point for a PV cell, as any other DC source, can be obtained by manipulating both voltage and current to maximize the power. It can be calculated according the PV cell characteristics curve, figure 2.9. It is only valid under a certain temperature and radiance [26].

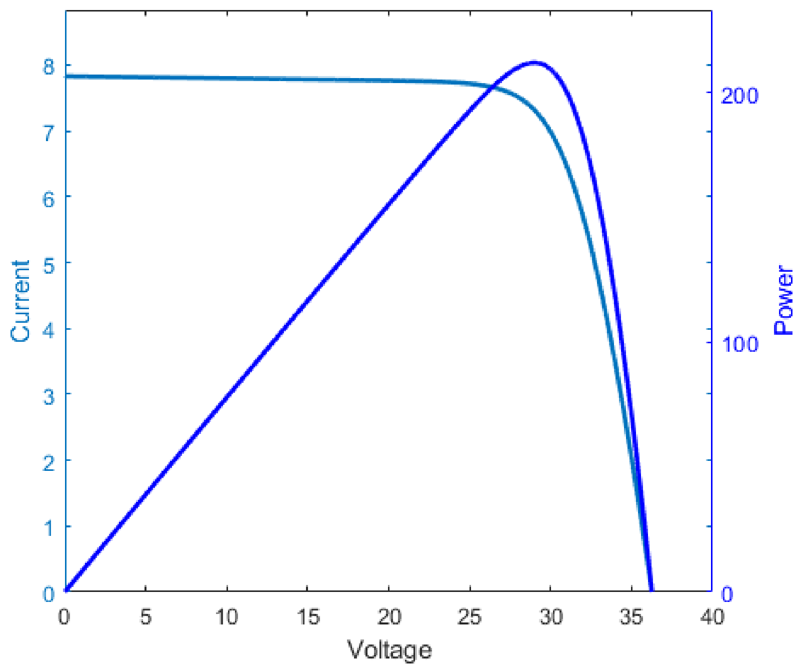

Figure 2.9: PV cell characteristic Curve. I-V curve on light blue and P-V curve on dark blue.

A MPPT method can be implemented either in software or hardware [25]. The authors in the last mentioned reference proposed a MPPT circuit hardware using the fractional open circuit voltage approach. Its theoretical principle is based on:

$$V_{mpp} = V_{OC}K(0 < k < 1) \tag{2.2}$$

The proposed circuit consisted of the MPPT control unit circuit and a MOSFET switch. The control unit, being a hysteresis voltage comparator, drives the MOSFET switch, generating control signals. It does so by comparing the MPP voltage and the voltage in the PV cell. The MOSFET switch gets the MPP by swinging around the required voltage range.

A MPPT method that does not take into account the charger efficiency can result in a lower value of transferred energy. A conventional MPPT method simply finds the point where the PV voltage is maximum ignoring the charger efficiency on that point. The authors in [22] proposed a MPPT design considering the charge efficiency. This method guarantees that the maximum power is delivered to the load instead of extract the maximum power from the PV cell.

There will be presented several different MPPT techniques:

- *1.Curve-Fitting Technique*: The Curve-Fitting Technique is based on mathematical equations and numeric expressions, used to predict the P-V characteristic curve:

$$P = aV^3 + bV^2 + cV + d \tag{2.3}$$

the parameters a, b, c and d are determined by sampling the PV voltage and power. Considering that at MPP:

$$\frac{dP}{dV} = 3aV^2 + 2bV + c \tag{2.4}$$

and

$$\frac{dP}{dV} = 0 \tag{2.5}$$

MPP can be calculated by:

$$V_{mpp} = \frac{-b \pm \sqrt{b^2 - 3ac}}{3a} \tag{2.6}$$

- *2.Fractional Short-Circuit Current (FSCI) Technique*: The MPP is characterized by its V_{mpp} and its I_{mpp}. If V_{mpp} and I_{mpp} are tracked, MPP can be tracked.

  Using this technique the V-I characteristic curve is predicted with mathematical equations or numerical approximations considering a range of environmental condition and degradation level of PV cells.

  Based on the V-I characteristics:

$$I_{mpp} \approx K_{sc} I_{sc} \tag{2.7}$$

  K_{sc} can be calculated considering the PV system at a various range of solar radiations and temperatures and usually varies between 0.64 and 0.85 [27].

- *3.Fractional Open-Circuit Voltage (FOCV) Technique*: This technique is very similiar to the FSCI Technique.

  V_{mpp} is calculated as follows:

$$V_{mpp} \approx K_{oc} V_{oc} \tag{2.8}$$

  Similarly to K_{sc}, $K_{oc}$is calculated by analysing the PV system at a various range of solar radiations and temperatures and varies between 0.78 and 0.92 [28].

- *4.Look-up Table Technique*: The Look-up Table technique makes use of the memory device of the MPPT control system. The MPP of the PV system is calculated in advance for each possible environmental conditions and it is stored in the memory device of the MPPT control system [29].

- *5.One-Cycle Control (OCC) Technique*: This technique is a non linear technique. The MPP can be calculated using a single-stage inverter. The output current of the inverter is adjusted according the voltage of the PV cell.

- *6. Differentiation Technique*: In this technique the MPP is calculated as follows:

$$\frac{dP}{dt} = \frac{d(IV)}{dt} = I\frac{dV}{dt} + V\frac{dI}{dt} = 0 \tag{2.9}$$

- *7. Feedback Voltage or Current Technique*: This technique is used when the system has no battery. Having no battery makes it simpler to calculate the MPP. The PV cell voltage/current is used to compare to a reference voltage/current previously calculated. The duty ratio of the dc/dc converter is adjusted to operate at the MPP or close to it.

- *8. Feedback of Power Variation With Voltage Technique*: The only difference between this technique and the Feedback Voltage Technique is in the ratio $\frac{dP}{dV}$. The maximum power control can be achieved if:

$$\frac{dP}{dV} = 0 \tag{2.10}$$

  Feedback control is powered by maximize the power at the load terminals.

- *9. Feedback of Power Variation With Current Technique*: This technique is similiar to the Feedback of Power Variation with Voltage Technique, the difference lies in the feedback.

- *10. Hill Climbing/Perturb and Observe*: These two techniques represent two different ways to execute the same fundamental method. The Hill Climbing technique requires a perturbation in the duty cycle of the DC/DC converter and the Perturb and Observe technique requires a small perturbation on the voltage of the PV cell. A perturbation on the duty cycle of the power converter disturbs the PV cell current and thus the PV cell voltage.

From the observation of the characteristic PV cell power curve, Figure 2.9, it can be concluded that the increment or decrement of the of the voltage increases or decreases the power when the point is on the left of the MPP and decreases or increases when the point is on the right. The idea is to repeat this method, periodically, until the MPP is obtained. Both techniques are susceptible to failure when the atmospheric conditions change abruptly.

The following figure represents the block diagram of the Hill Climbing technique.

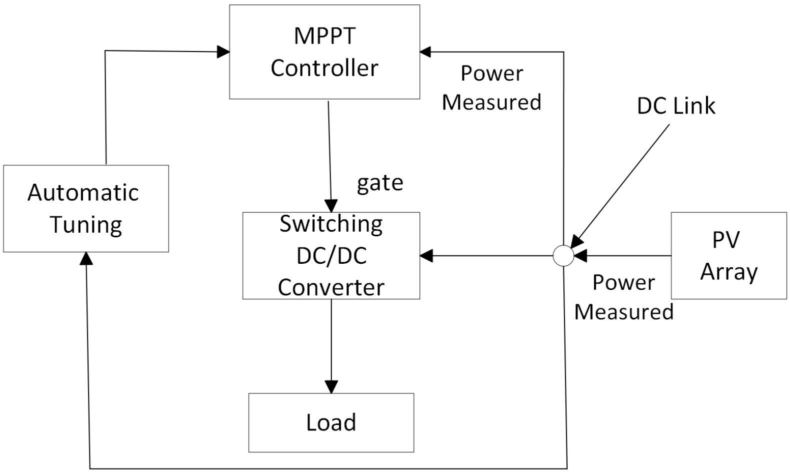

Figure 2.10: Block diagram from Hill Climbing Technique. Adapted from [29].

- *11. Incremental Conductance (Inc-Cond) Technique*: Considering the derivative of the cell output power with its voltage is given by:

$$\frac{dP}{dV} = \frac{d(IV)}{dV} = I + V\frac{dI}{dV} = I + V\frac{\Delta I}{\Delta V} \tag{2.11}$$

and that at MPP:

$$\frac{dP}{dV} = 0 \tag{2.12}$$

the derivative of the cell output power with its voltage can be rewritten as:

$$\frac{\Delta I}{\Delta V} = \frac{-I}{V}, \quad at \quad MPP. \tag{2.13}$$

$$\frac{\Delta I}{\Delta V} > \frac{-I}{V}, \quad at \quad left \quad of \quad MPP. \tag{2.14}$$

$$\frac{\Delta I}{\Delta V} < \frac{-I}{V}, \quad at \quad right \quad of \quad MPP. \tag{2.15}$$

- *12. Forced Oscillation Technique*: In this technique a small signal sinusoidal perturbation is injected into the switching frequency and then the AC component is compared to the average value of the cell terminal voltage.

- *13. Ripple Correlation Control (RCC) Technique*: In this technique, the current ripple of the PV cell is used by the PV system to execute MPPT. There is no need for an external perturbation since the ripple is a result of using a switching converter.

The RCC technique correlates $\frac{dp}{dt}$ with either $\frac{di}{dt}$ or $\frac{dv}{dt}$, as follows:

$$\frac{dv}{dt} > 0 \quad or \quad \frac{di}{dt} > 0 \quad and \quad \frac{dp}{dt} > 0 \implies V < V_{mpp} \quad or \quad I < I_{mpp} \tag{2.16}$$

$$\frac{dv}{dt} > 0 \ \ or \ \ \frac{di}{dt} > 0 \ \ and \ \ \frac{dp}{dt} < 0 \implies V > V_{mpp} \ \ or \ \ I < I_{mpp} \tag{2.17}$$

The purpose of this method is to force the current ripple to be zero and consequently achieve MPP.

- *14. Current Sweep Technique*: As its names suggests, this technique uses a sweep waveform for the PV cell current so that the I-V characteristic of the PV cell can be obtained. The V_{mpp} can then be calculated considering the characteristic curve at the same interval.

The function for the current sweep is given by:

$$i(t) = k_1 \frac{di}{dt} \iff i(t) = k_2 \, e^{\frac{t}{k_1}} \tag{2.18}$$

Being k_2 taken as I_{mpp} at MPP. Once more at MPP:

$$\frac{dp(t)}{dt} = \frac{d(v(t)i(t))}{dt} = i(t)\frac{dv(t)}{dt} + v(t)\frac{di(t)}{dt} = 0 \tag{2.19}$$

Using (2.18):

$$\frac{dp(t)}{dt} = \left(k_1 \frac{dv(t)}{dt} + v(t)\right) \frac{di(t)}{dt} = 0 \tag{2.20}$$

The reference point is adapted in a fixed time interval. The results of this technique are precise if proportionality coefficients k_1 and k_2 are chosen.

- *15. Estimated-Perturb-Perturb (EPP) Technique*: This technique is an extended PO method. It has one estimate mode between two perturbation modes.

The perturbation process searches over the nonlinear PV characteristic. The estimate process compensates for the perturbation process, considering irradiance changing conditions.

- *16. Parasitic Capacitance Technique*: This technique resembles to the Inc-Con Technique. The difference here is that the PV cells parasitic junction capacitance C_p is considered.

The capacitance can be considered by making a small change in the PV cell model equation:

$$I = I_{pv} - I_o \left[exp \left(\frac{V + IR_s}{aV_t} \right) - 1 \right] - \frac{v + IR_s}{R_{sh}} + C_p \frac{dv}{dt} \tag{2.21}$$

This equation can be rewritten as:

$$I = f(v) + C_p \frac{dv}{dt} \tag{2.22}$$

where:

$$f(v) = I_{pv} = I_o \left[exp \left(\frac{V + IR_s}{aV_t} \right) - 1 \right] - \frac{v + IR_s}{R_{sh}} \tag{2.23}$$

The Power output from the PV cell is given by:

$$P = V(f(v)) + C_p \frac{dv}{dt} \tag{2.24}$$

Considering, once more, that the MPP is located where $\frac{dP}{dV} = 0$:

$$g_p = \frac{df(v)}{dv} + C_p \left(\frac{\dot{V}}{V} + \frac{\ddot{V}}{\dot{V}} + \frac{f(v)}{dV} \right) \tag{2.25}$$

where $\frac{df(v)}{dv}$ represents the instantaneous conductance, $C_p(\frac{\dot{V}}{V} + \frac{\ddot{V}}{\dot{V}})$ the incremental conductance and $\frac{f(v)}{dv}$ the induced ripple from the parasitic capacitance.

The cell conductance is the ratio of the instantaneous cell current to the instantaneous cell voltage:

$$g_p = \frac{P_{gp}}{V_o^2} \tag{2.26}$$

where P_{gp} is the average ripple power and V_o is the magnitude of the voltage ripple and are obtained from a circuit configuration, as can be seen in Figure 2.12.

The inputs to the previous circuit are the PV cell current and voltage. The high-pass (HP) filters remove the DC component of V. The multipliers generate the AC signals of V_o^2 and P_{gp}, and both are then filtered by the low-pass (LP) filters.

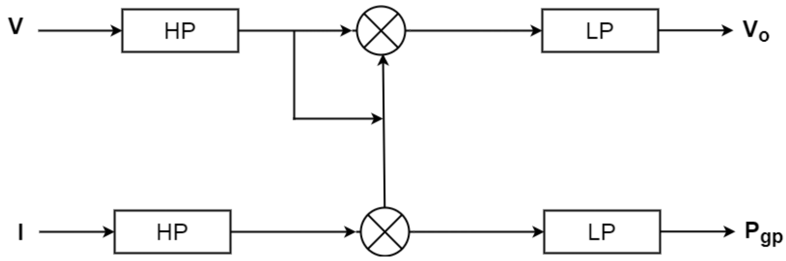

Figure 2.11: PV Array connected to boost circuit in RCC technique. Adapted from [29].

- *17. Load Current/Load Voltage Maximization Technique*: When there is a direct connection to the load, it cannot be guarantee the PV system is operating at the MPP. In conclusion, execution at the MPP cannot be attained using a tunable matching network that interfaces the load to the PV cell. The principal components of the MPPT circuit are the power stage and the controller. The power stage is executed with a switched mode power converter, thus the control input is the duty cycle.

- *18. DC Link Capacitor Droop Control Technique*: This technique is design to work with a PV system that is connected in parallel with an AC system.

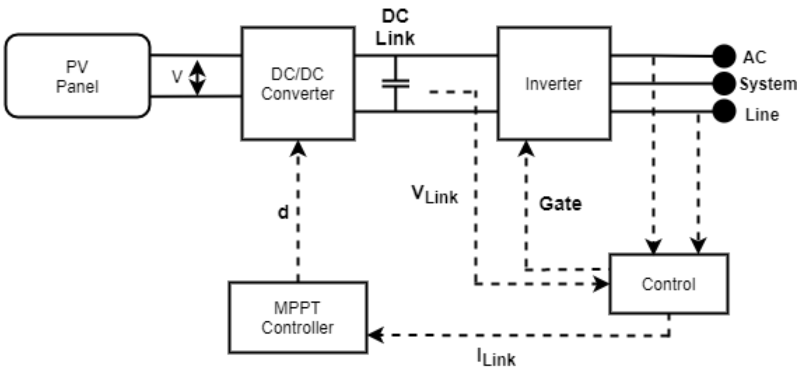

Figure 2.12: Block diagram of DC link capacitor droop technique. Adapted from [29].

Considering that the duty cycle (d) of an ideal boost converter is given by:

$$d = 1 - \frac{V}{V_{link}} \tag{2.27}$$

Where V is the voltage across the PV cell and V_{link} is the voltage across the dc link.

When V_{link} is constant, it is possible to increase the output power of the converter by increasing the maximum power available from the PV cell and, while the current is increasing, V_{link} can be kept constant. Otherwise V_{link} starts drooping. Just before the drooping point, the current control of the inverter is at its maximum and the PV cell operates at MPP.

- *19. Linearization-Based MPPT Technique*: In this technique the MPP is calculated using a set of linear equations, considering the relation between the values of voltage and current at the MPP.

  The relation between voltage and current tends to be linear for higher irradiation conditions. That is due to the effects of the PV cell resistance. The MPP is obtained considering the relation of voltage and current.

- *20.Intelligence MPPT Techniques*: These techniques attained very good performances and fast responses with no overshoot.

  - *a. Fuzzy Logic (FL)-Based MPPT Technique*: FL-based MPPT technique does not require the knowledge of the PV model. This method has two inputs and one output. The two input variables are error(e) and change in error (C_e) and are given by:

$$e(k) = \frac{dP}{dV}(k) = \frac{dP}{dV}(k-1) \tag{2.28}$$

$$C_e(k) = e(k) - e(k-1) \tag{2.29}$$

  - *b. Artificial Neural Network (ANN)-Based MPPT Technique*: The control on this technique is like a black box model and thus, does not require detail information about the PV system.

    For MPPT, the ANN input can be the PV voltage or current of the PV cell, irradiance or temperature, and the output is the identified maximum power or the duty cycle signal that is used so the converter operates at the MPP. Once the relation of V_{mpp} with temperature and irradiance is known, ANN method is capable of tracking the MPP online.

  - *c. Particle Swarm Optimization-Based MPPT (PSO-MPPT) Technique*: There is a possibility of multiple maxima in the P-V characteristic curve being found for partial shading condition when the PV system is composed of multiple PV arrays. The PSO technique is efficient in multivariable problem and thus it is used for multi-PV array structure.

- *21. Sliding-Mode-Based (SMB) MPPT Technique*: Considering a variable h, a constant term defined as $h = \frac{I}{V} + \frac{\Delta I}{\Delta V} V$. At MPP, h=0. This notion is used in SMB MPPT technique. The dc/dc converter is designed such the switching control(u) is given by:

$$u = 1, h < 0 \tag{2.30}$$

$$u = 0, h \geqslant 0 \tag{2.31}$$

when u=0, the converter-switch is open and when u=1, the converter-switch is closed. This is a way to force the converter to operate at MPP.

- *22. Gauss-Newton Technique*: This technique is the fastest algorithm. It is used a root finding algorithm.

  Using this technique, the two first derivates of change in power estimate the direction and number of iteration of convergence:

$$v(k+1) = v(k)\frac{\frac{dp}{dv}|_{v=v(k)}}{\frac{d^2p}{dv^2}|_{v=v(k)}} \tag{2.32}$$

- *23. Steepest-Descent Technique*: The nearest local MPP is calculated using:

$$\frac{\frac{dp}{dv}|_{v=v(k)}}{K_\varepsilon} \tag{2.33}$$

  Where K_ε is the step size corrector. And:

$$\frac{dp}{dv} = f(v, p) \tag{2.34}$$

$$f(v(k), p(k)) = \frac{p(k+1) - p(k-1)}{2\Delta V} + O(\Delta V^3) \tag{2.35}$$

  Where $O(\Delta V^3)$ is the local truncation error for centered differentiation.

- *24. Analytic-Based MPPT Technique*: In this technique, observations and experimental results play a crucial roll. V_{oc} and I_{sc} values are observed and considering those values, a ball of small radius ε is picked for each panel, so the MPP is inside the ball. This technique is based on the mean value theorem. This means MPP is acquired from that ball, considering the mean value theorem.

- *25. Hybrid MPPT (HMPPT) Techniques*: In the MPPT Technique, membership functions and control are optimized by the genetic algorithm. Hybrid control techniques are essential to control the perturbation size.

The following figure is an example of a proposed hybrid MPPT technique with PO and ANN techniques:

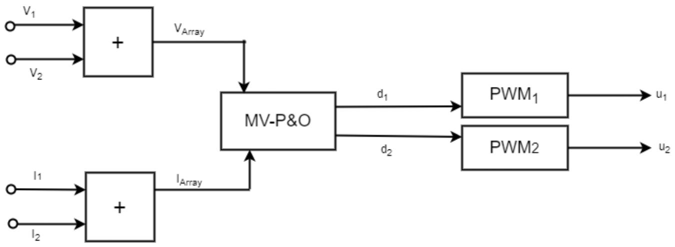

Figure 2.13: Multivariable PO structures. Adapted from [29].

- *26. MPPT Techniques for Mismatched Conditions*: In the same PV field it is possible to have Pv modules with different orientations. There is also very common to have manufacturing tolerances, non-uniformity of ambient temperature close to the panel due to irregular solar irradiation and air circulation or dust.

  Mismatched conditions can make the energy productivity drop to 20% of the not mismatched strings. Mismatched can also influence the P-V characteristic of the PV field to have more than one peak. Distributed Maximum Power Point Tracking (DMPPT) can reduce the mismatched problems, due to the use of a MPPT for each module. DMPPT guarantees higher energy efficiency than other methods, when there are mismatching conditions.

Most MPPT techniques do not take into account the power being transferred and stored on the power converter. These techniques maximize the power point but do not guarantee that the power transferred it is also the maximum.

Table 2.2: Comparison of different MPPT techniques according to their classified types [29].

MPPT Technique	Control Strategy	Control Variable	Circuitry (A/D)	Parameter Tuning	Cost	Complexity Level	Applications	Converter Used (DC/DC or DC/AC)
1	INC [1]	V [2]	D [3]	yes	INEX [4]	Simple	Stand-alone	DC/DC
2 e 3	INC	V or I [5]	Both	yes	INEX	Simple	Stand-alone	DC/DC
4	INC	V, I	D	yes	INEX	Simple	Stand-alone	DC/DC
5	SM	I	Both	yes	INEX	Simple	Grid	DC/AC
6	SM [6]	V or I	D	yes	EX [7]	Complex	Stand-alone	DC/DC
7	SM	V or I	Both	no	INEX	Simple	Stand-alone	Both
8	SM	V, I	D	no	EX	Complex	Stand-alone	Both
9	SM	V, I	D	no	EX	Medium	Stand-alone	Both
10	SM	V, I	Both	no	EX	Complex	Stand-alone	DC/DC
11	SM	V, I	D	no	EX	Complex	Stand-alone	DC/DC
12	MM [8]	V or I	A [9]	yes	EX	Complex	Stand-alone	DC/DC
13	MM	V or I	A	yes	EX	Complex	Stand-alone	DC/DC
14	MM	I	D	yes	EX	Complex	Grid	DC/AC
15	SM	V, I	Both	no	EX	Complex		DC/DC
16	SM	V, I	D	yes	EX	Simple	Stand-alone	Both
17	MM	V	A	no	INEX	Medium	Stand-alone	DC/DC
18	MM	V	Both	yes	EX	Simple	Grid	Two stages DC/DC + DC/AC
19	SM	Irradiance	D	yes	INEX	Medium	Stand-alone	DC/DC
20	INT [10]	V or I	D	yes	EX	Medium	Both	Both
21	SM	V or I	D	no	EX	Complex	Both	Both
22	SM	V or I	D	no	EX	Simple/ Medium	Stand-alone	DC/DC
23	SM	V or I	D	no	EX	Medium	Stand-alone	DC/DC
24	INC	V or I	Both	yes	EX	Medium/ Complex	Stand-alone	DC/DC
25	SM	V or I	D	yes	EX	Medium/ Complex	Both	Both
26	INT	V or I	D	yes	EX	Medium	Both	Both

[1] Indirect control; [2] Voltage [3] Digital [4] Inexpensive [5] Current [6] Sampling Method [7] Expensive
[8] Modulation Method [9] Analog [10] Inteligent or Probabilistic Control

Chapter 3

Proposed Power Conditioning

The power conditioning phase is one of the most important phases of an energy harvesting system for indoor applications since the amount of power extracted is usually very low and there is a need to step it up. Consequently, it is crucial to gain insight on this matter. Specifically the goals for this chapter are as follows:

- Study the influence of a SC on an energy harvesting system;
- Study the most appropriate SC for this project;
- Develop a model for the SC DC-DC voltage doubler and validate such model through simulation;
- Develop a model for an Undervoltage Lockout Circuit (ULC) and validate such model through simulation.

As explained in section 2.2, a DC-DC switched converter is typically used to deliver a higher voltage than the provided voltage supply and thus ideal to process the electricity from the PV system and boost it. The power loss of this type of converters are mainly dynamic and resistive, the first due to the switching frequency and the parasitic capacitance of the converter, and the second one due to the value of the resistance of the converter being finite. Considering this, extra caution is needed when choosing the clock frequency, never forgetting that a higher frequency might result on a decrease of the output power. For this work, a charge pump with a voltage doubler topology is the most suitable option. The voltage doubler typology has an important advantage for its boosting low voltages. Considering that the voltage drop is never higher than the supply voltage, it is possible to use MOS transistors with low voltage, appropriated for this kind of project, when the amounts of energy are low.

3.1 Cross Couple Voltage Doubler Charge Pump

The proposed system is a cross coupled voltage doubler. A very good option when the supply voltages are low.

The body connection of each transistor proved to be a crucial point for the charge pump. The body in the N-channel metal-oxide semiconductor (NMOS) transistors need to be connected to either ground or a power source, as all the NMOS transistors share a common substrate that can only be biased to one voltage. In the case of the PMOS transistors, the body should be at an equal or higher voltage than the source. Originally, the body was connected to the source, but initial simulations failed to converge, due to an inversion on the substrate diodes of the PMOS transistors, showing that this was not the best option. These results lead to a new approach, adding two extra PMOS transistors. The final Charge Pump design can be seen in Figure 3.1 and the extra devices are marked as bulk bias.

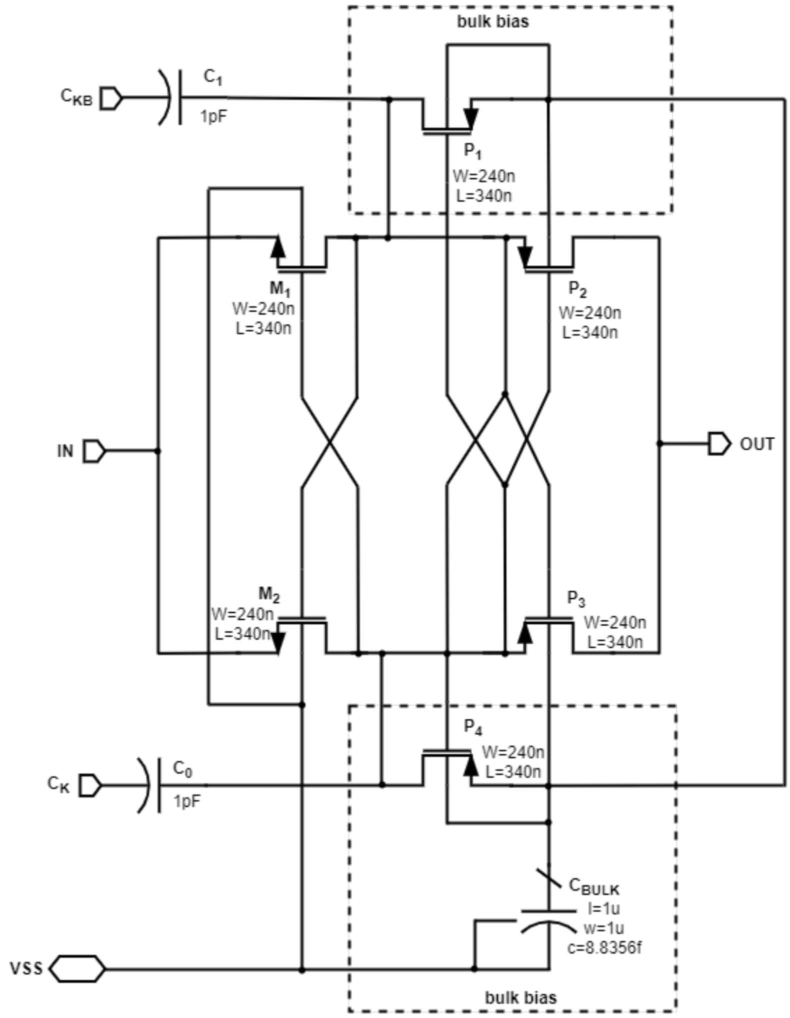

Figure 3.1: Proposed Charge Pump Design

The modifications on the original design were made to prevent an inversion of the PMOS substrate diodes and guarantee that the voltage in the body is the higher value between the drain voltage and the source voltage. New simulations proved this approach solved the initial problem with the substrate diodes of the PMOS transistors. The sizing parameters of the transistors are the minimum for the type of transistors chosen for the design.

A test bench was created in order to analysed the performance of the charge pump. The test bench used can be seen in Figure 3.2. The input voltage selected was 1 V. The ideal frequency for the clocks (f_{CK}) was studied throughout various simulations. In the output of the Charge Pump a load resistance and a load capacitance were added, later replaced with a supercapacitor, as discussed in Chapter 4. The load resistance (R_{Load}) has no fixed value, it shifts as desired to achieve a certain value of output voltage and power. This value was determined after simulations, being the maximum value that guarantees the correct operation of the circuit. The value used for the load capacitance was 10 pF. The test bench also includes a ring oscillator between the clock and the charge pump and an input voltage controller.

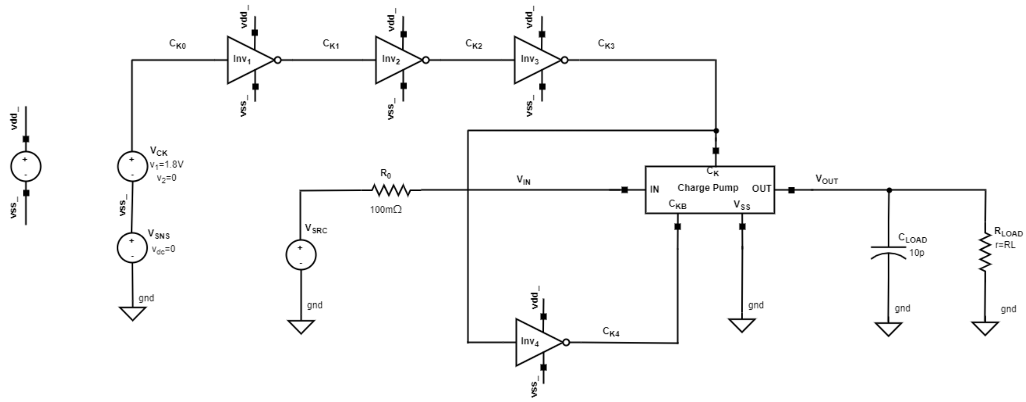

Figure 3.2: Charge Pump test bench

3.1.1 Charge Pump Performance Analysis

Several simulations were carried out to correctly evaluate the performance of the converter and to study what could be improved. The values of Output Voltage (V_{OUT}), Power Voltage (P_{OUT}), Output Current (I_{OUT}) were analyse and than the value of the input power (P_{IN}) was extracted. P_{IN} is the sum of the power in the source ($P_{INsource}$) and the power in the supply ($P_{INsupply}$), since the two values influence the resulting efficiency (eff) of the overall circuit and both are considered when calculating it.

The efficiency of the charge pump was determined with the following equation:

$$eff = \left(\frac{P_{OUT}}{P_{INsource} + P_{INsupply}}\right) \times 100 \tag{3.1}$$

Firstly, the performance of the charge pump was analysed varying R_{Load} and having a fixed value for f_{CK} of 550kHz. The results are shown in Figure 3.3. The analysis performed was a Periodic Steady State Analysis (PSS) and shows the response of each parameter.

Observing the graphics, it can be concluded that the results are optimal for a lower R_{Load} value, as it was expected. Both output voltage and current achieve a stable value when the R_{Load} is approximately 25MΩ, stabilizing at 3.04V, being this the maximum value for V_{OUT}, and 27.65nA. Although the output power stabilizes according to V_{OUT}, the steady value of P_{OUT} is not its optimal

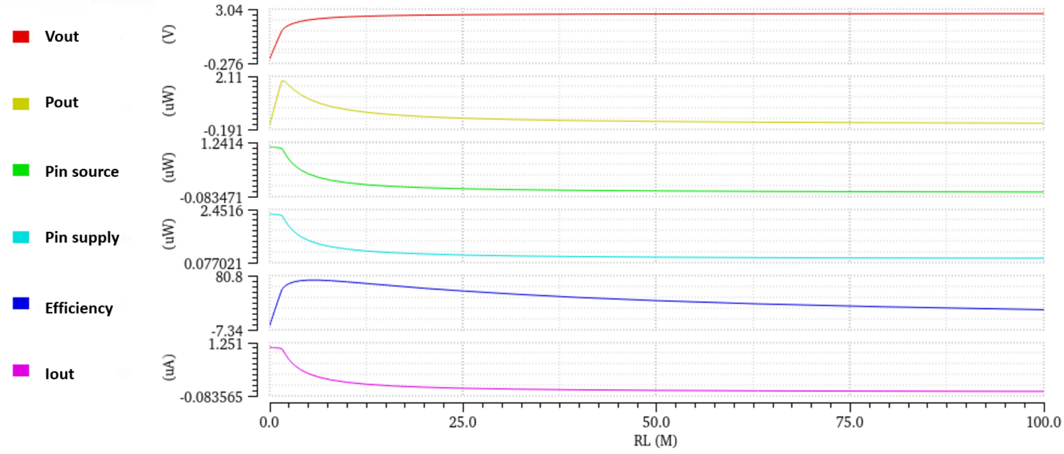

Figure 3.3: Charge Pump Performance Analysis with $f_{CK} = 550kHz$

value since the maximum power is achieved when R_{Load} is 1.6MΩ. Considering the efficiency obtained at the peak, 73.44%, when R_{Load} is approximately 6.31MΩ, it can be said that the results were satisfactory but it was possible to improve them.

Once it was recognized the optimal value for the R_{Load}, a new simulation was performed, this time varying the f_{CK} and having the fixed value of 6.31MΩ for the R_{Load}. The results of the PSS analysis can be seen in Figure 3.4.

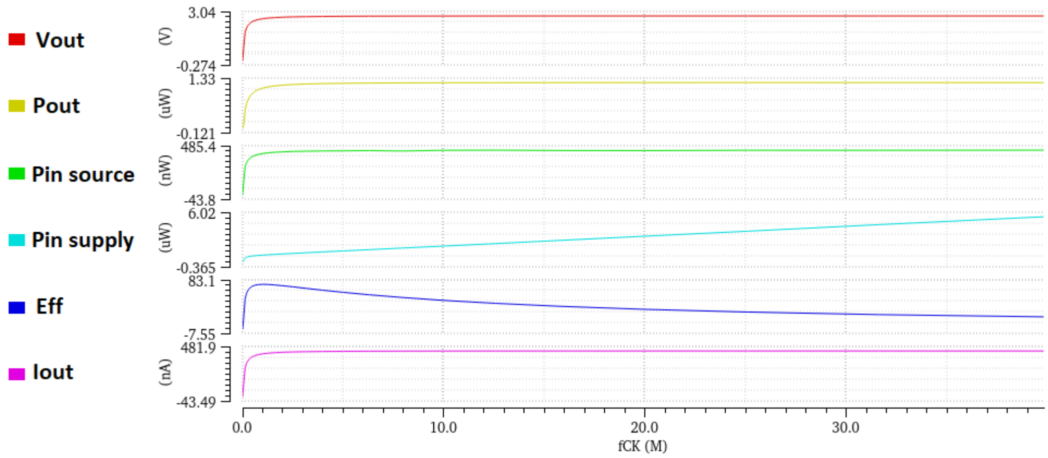

Figure 3.4: Charge Pump Performance Analysis with $R_{Load} = 6.31M\Omega$

In contrast to what happened in the previous simulation, with a fixed value for R_{Load}, the behaviour of P_{OUT} is similar to V_{OUT} and I_{OUT} since the three parameters achieved a steady state and maximum value at the same point when f_{CK} is around 5MHz. The efficiency peak rised to 75.55%, with f_{CK} at 1MHz. It can be observed that a variation on the clock frequency has a bigger impact on the input power in the supply, as this value increases as f_{CK} increases.

Fixing the value of f_{CK} at 1MHz and varying once again R_{Load}, new simulations were performed. The results of the PSS analysis are shown in Figure 3.5.

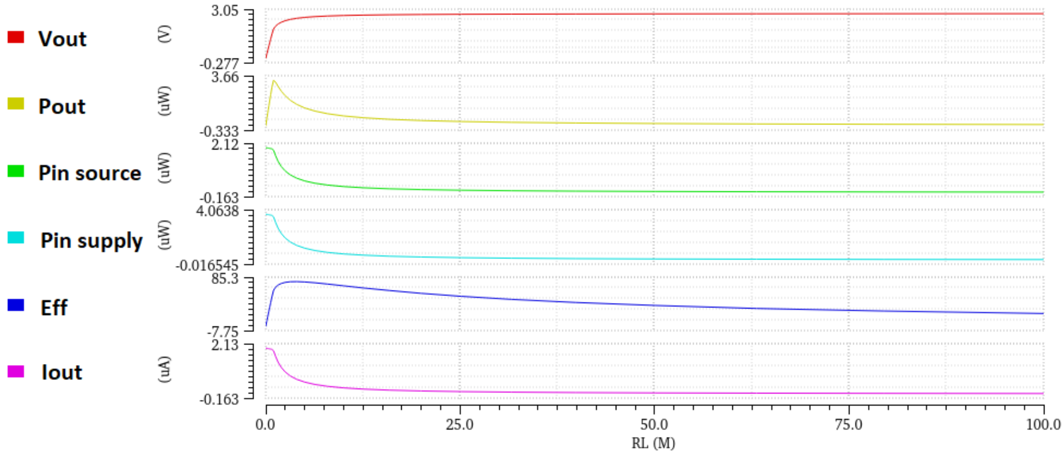

Figure 3.5: Charge Pump Performance Analysis with $f_{CK} = 1MHz$

The behaviour of each parameter for this simulation is close to what was obtained in the first simulation, with a fixed value of 550kHz for f_{CK} and varying R_{Load}. The output power steady state does not correspond to the maximum power point, but when $R_{Load} = 1M\Omega$, achieving 5.33uW, much higher than the steady state value of 90nW. Regarding the efficiency, a new peak was achieved at 77.34%, with $R_{Load} = 3.2M\Omega$.

In the last simulation performed regarding the analysis of the charge pump, the value of R_{Load} was once again fixed, at the new peak of 3.2MΩ. The results of the PSS analysis are shown in Figure 3.6.

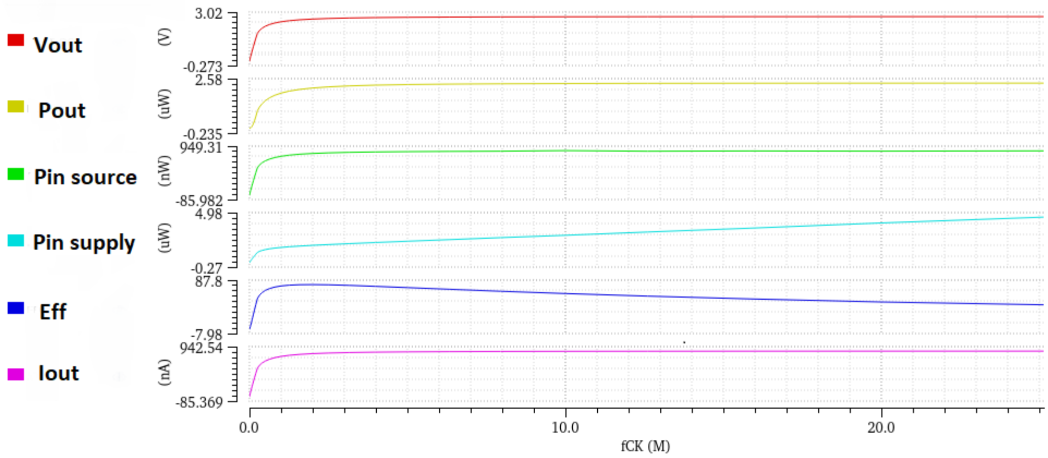

Figure 3.6: Charge Pump Performance Analysis with $R_{Load} = 3.2M\Omega$

Considering the results of this last simulation, it can be said that the behaviour of the system is very satisfactory, being achieved an approximate efficiency of 80%. Thus, the chosen design of the charge pump is suitable for the system aimed to develop as the main goals were for the charge pump to boost the voltage it receives and transfer the maximum amount of power. It is capable to boost the voltage it receives and deliver a very reasonable percentage of that power to the load.

The results of the transient analysis for V_{OUT} and P_{OUT} with $R_{Load} = 3.2M\Omega$ and $f_{CK} = 1M\Omega$ can be seen in Figure 3.7.

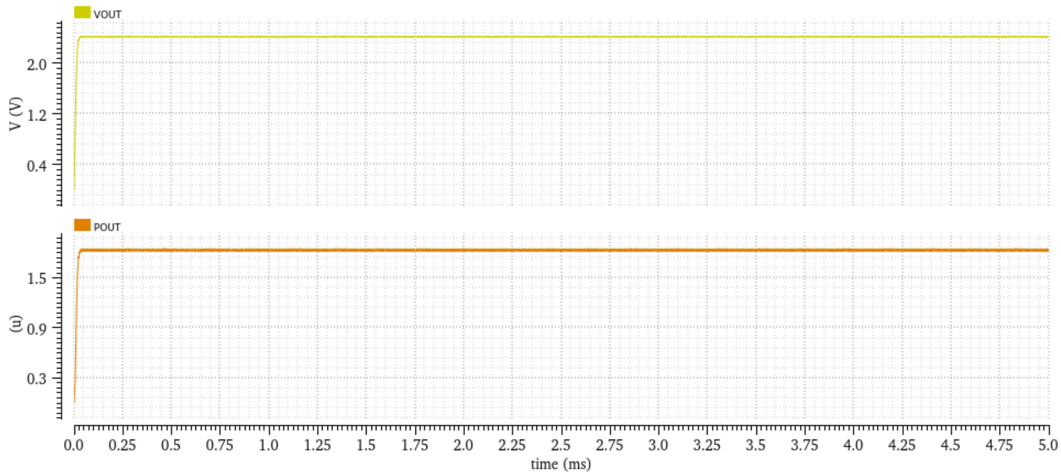

Figure 3.7: Charge Pump Performance Analysis with $R_{Load} = 3.2M\Omega$

3.2 Undervoltage Lockout Circuit

One important goal of this PV system is to guarantee that the charge pump does not start working when there is not enough energy for a correct operation. Not having the necessary energy would lead to **cold booting**. This phenomenon is all the useless rebooting cycles of the system when there is not enough energy stored to achieve the threshold voltage at which the system can operate properly (*i.e.* the startup or "wake up" voltage for all the relevant circuits to begin operating nominally). If the voltage is too low, the transistors may be switched and the wrong voltage could be produced. Thus, it was necessary to guarantee the converter would only work when the input voltage was sufficient, avoiding constant rebooting cycles.

This goal was achieved creating an ULC to place between the PV cell and the charge pump. This circuit will disable the system when the supply voltage is below the minimum value that allows the correct functioning by activating the system only once that minimum value is achieved. The model used consists on a voltage divider, a reference voltage (V_{REF}) cell, a comparator and a pass transistor and can be seen in Figure 3.8.

The voltage divider consists on four PMOS transistors with the same length and width. On point A, the voltage is equals to V_{DD}, on point B it is half of V_{DD}, on point C it is a third of V_{DD} and on point D it is a quarter of V_{DD}. The comparator selects the value of V_{SMP} when it is bigger than V_{REF}. V_{REF} is a fixed value of 376mV. This value was the optimal value obtained on simulations. The idea was that the comparator turned on when $1/4 \times V_{DD} = V_{REF}$, but the simulations showed the comparator allows a wider range, enabling at 800mV, as is shown in Figure 3.9, which is significantly lower than $4 \times V_{REF}$, but sufficient for a correct operation of the charge pump.

The reference voltage is secured by the V_{REF} cell, as it can be seen in Figure 3.10.

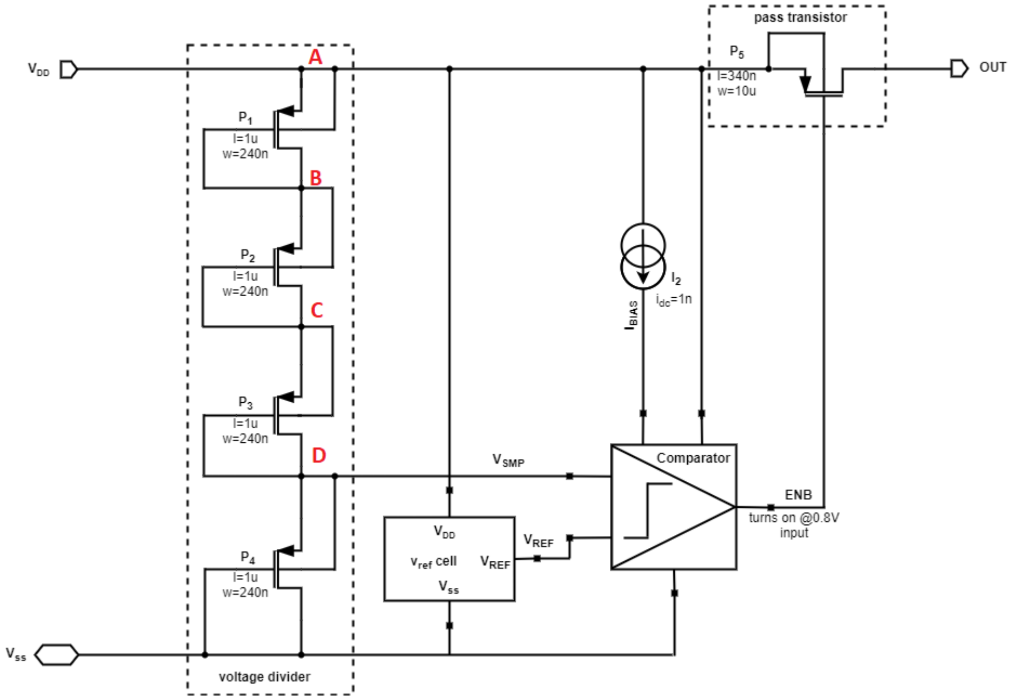

Figure 3.8: Undervoltage Lockout Circuit

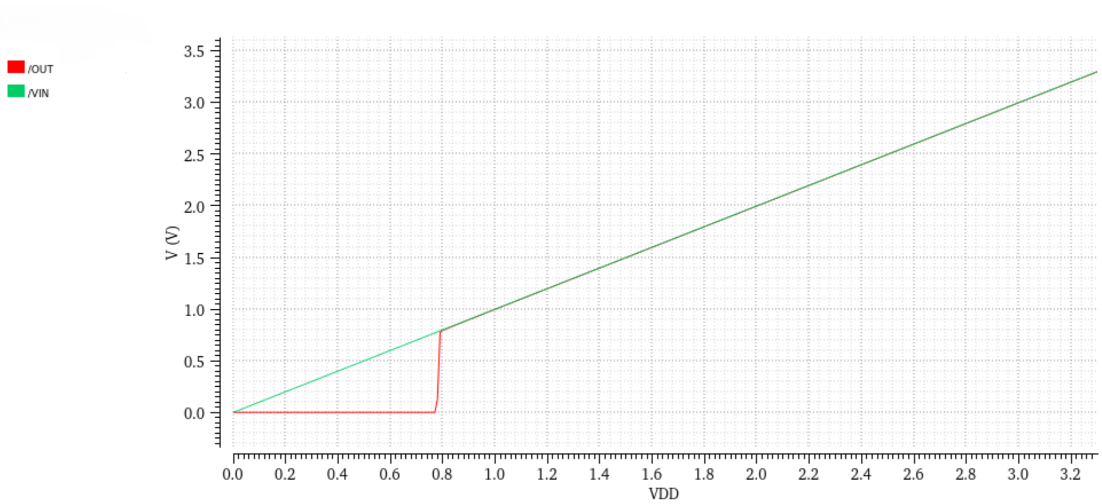

Figure 3.9: Output Enabling

This cell was conceived to maintain a fixed value of the voltage supply even considering this parameter has variations. As explained before, this circuit needs a threshold voltage to trigger its correct operation. The V_{REF} cell delivers this value. When V_{SMP} is higher than the V_{REF} nominal, 376mV, it will be selected by the comparator and, once it is equal or greater than 800mV, it will turn on the enable.

The design used for the comparator can be seen in Figure 3.11.

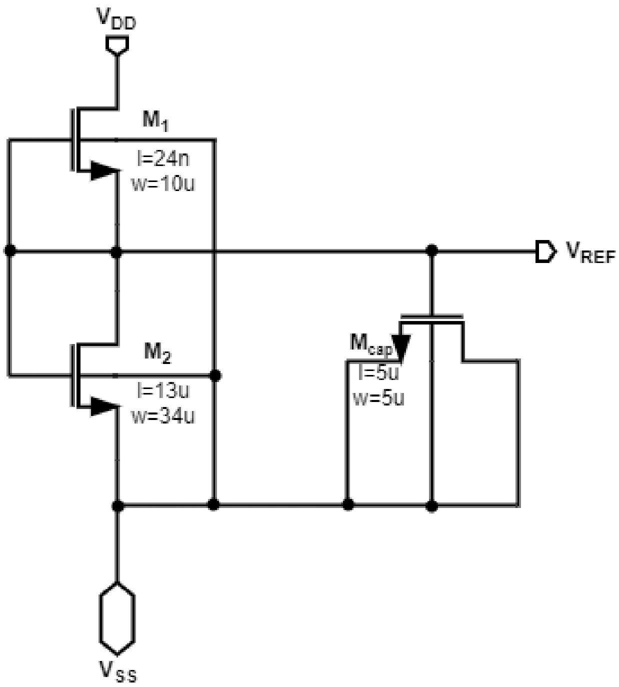

Figure 3.10: V_{REF} cell

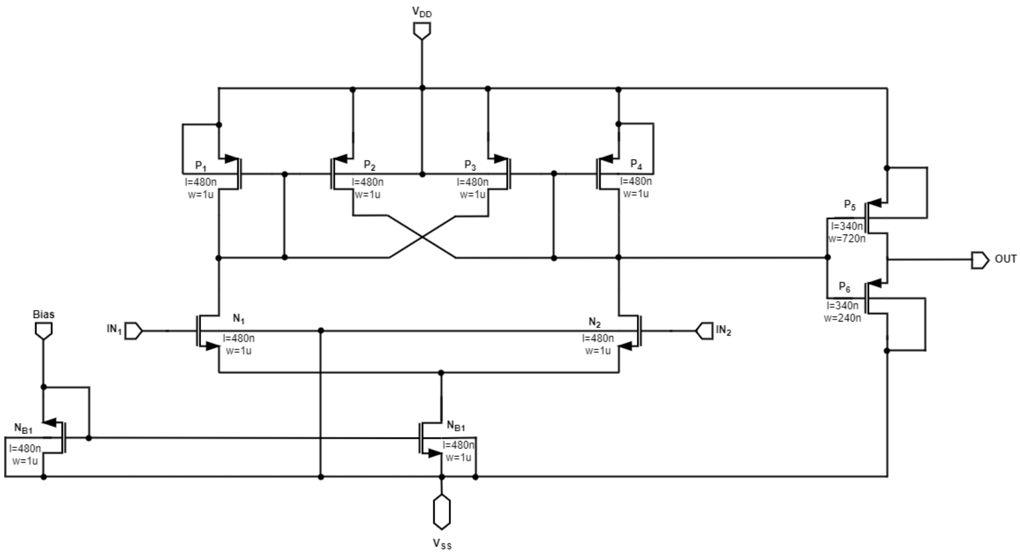

Figure 3.11: Comparator model

3.3 Power Conditioning Complete Stage

The final circuit for the power conditioning stage is presented in Figure 3.12.

The ULC between the voltage source and the charge pump was placed to guarantee that the converter only operates when there is enough voltage for its correct operation. New simulations were performed to study if the charge pump would operate correctly when the ULC was added. The results are show in Figure 3.13.

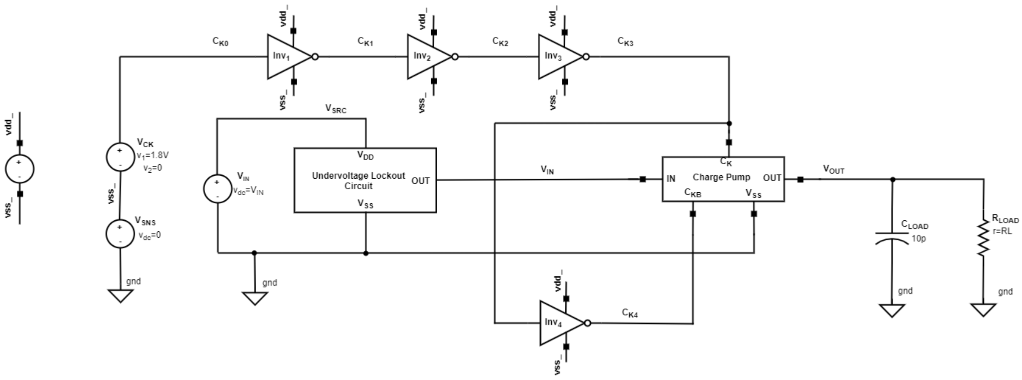

Figure 3.12: Power Conditioning Circuit Test Bench

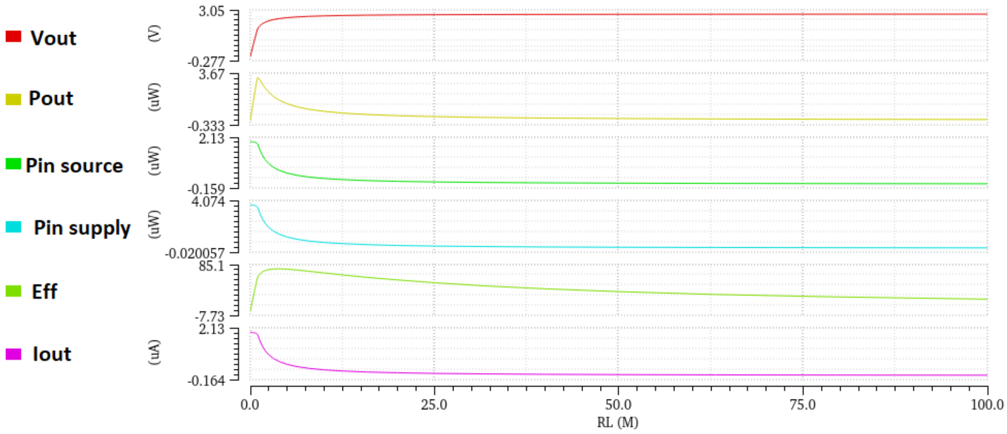

(a)

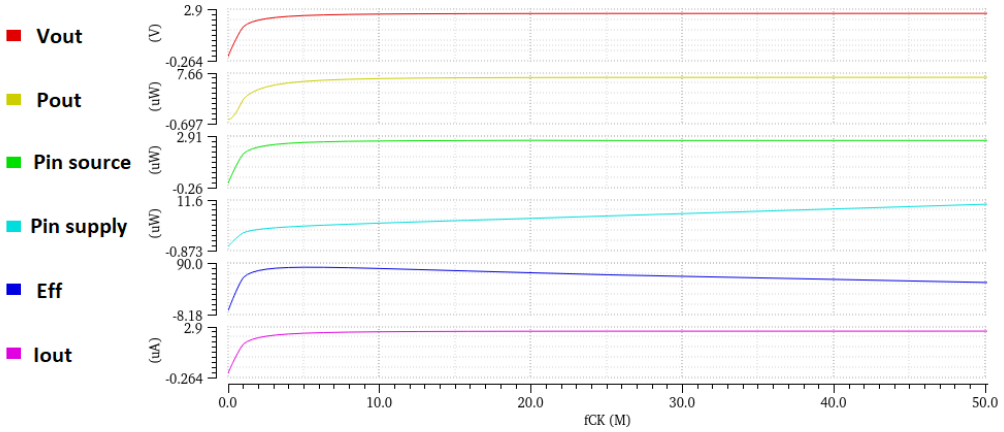

(b)

Figure 3.13: Power Conditioning Circuit Analysis (a) with $f_{CK} = 1MHz$ and varying R_{Load} (b) with $R_{Load} = 1M\Omega$ and varying f_{CK}

Analysing the simulations results, it was concluded that the charge pump works properly when the UCL was added.

In the first simulation, with $f_{CK} = 1MHZ$ and varying the R_{Load} value, an efficiency of 77.41% was obtained when $R_{Load} = 3.98M\Omega$, a similar result to what was obtained in the charge pump performance simulations. Naturally, there is a decrease in both the P_{OUT} and the efficiency as

R_{Load} increases.

When fixing the R_{Load} in 1MΩ and varying f_{CK}, the results are slightly better, achieving an efficiency of 81.78%. The results of the transient analysis for V_{OUT} and P_{OUT} with $R_{Load} = 3M\Omega$ and $f_{CK} = 1M\Omega$ can be seen in Figure 3.14. An efficiency of 78.03% was achieved.

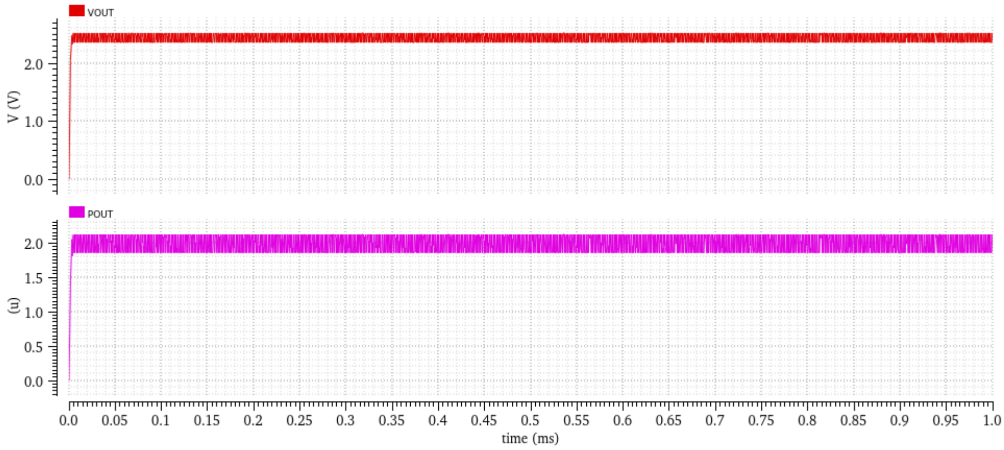

Figure 3.14: Power Conditioning Stage Transient Analysis

Analysing all the simulation results for the Power Conditioning stage, it is safe to consider that the first goal of this dissertation was achieved as the charge pump served its purpose of boosting the input voltage and deliver a very satisfactory percentage of the resulting power to the load.

Chapter 4

Photovoltaic System - Proposed Approach

This chapter presents an overview of the proposed PV system. The model presented aims to achieve the maximum power point and best efficiency possible. The goals for this chapter are as follows:

- Study the influence of a PV cell;
- Study the influence of a supercapacitor;
- Evaluate the performance of the developed system through simulation.

The main goal of the presented system is to maximise the power being delivered to the load and consequently attain an optimal efficiency and implement an efficient energy storage element.

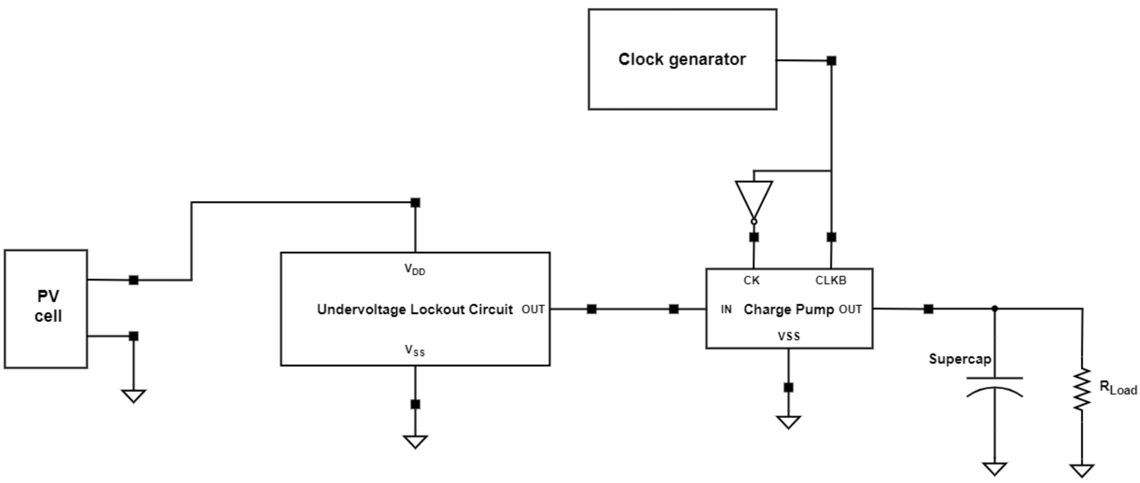

Figure 4.1: PV system overview

4.1 The Photovoltaic Cell

Nowadays, the most common way to simulate the behaviour of a PV cell is through an equivalent circuit [30]. The main issue on using an equivalent circuit relies on the parameters extraction since all of the parameters required to define the behaviour of a PV cell have to be estimated correctly to obtain a good fitting for the I-V curve of the PV cell. There are several ways to extract these parameters depending on the information available which in most cases are the voltage and current on characteristic points, such as the short circuit current, I_{sc}, the MPP voltage and current, V_{MPP} and I_{MPP} and the open circuit voltage V_{OP}.

To design a PV cell is necessary to choose a suitable model for the purpose of the system. Based on equation 4.1, a model was developed.

$$I = I_{SC}\frac{1-\left(\frac{V}{V_{OC}}\right)^{k}}{1+h\left(\frac{V}{V_{OC}}\right)} \tag{4.1}$$

Where I_{SC} is the short cut current and V_{OC} is the open circuit voltage.

The PV cell used in this work is modeled in verilogA. Refer to Appendix A to see the VerilogA function.

4.2 The Supercapacitor

The energy storage element has a crucial role on a PV system since it ensures that it will be a continuous supply, even if there is no sufficient power being harvest by the PV cell, this component should ensure the system keeps working. After studying the various storage elements, their behaviour, advantages and disadvantages, the supercapacitor was considered the most suitable option for the system aimed to implement, mainly for its smaller size when compared to a typical battery. Supercapacitor sizing in microsystem can go to the range of hundreds and thousands of faraday. For the proposed system it is not justified to have such a big capacitor in the load as the amount of power to be buffered is small.

4.3 PV System Performance Analysis

As explained in the previous chapter the initial simulations were made considering only the power conditioning stage, using a simple voltage control as the input voltage source instead of the PV cell and a small capacitor and load resistance in the energy storage stage. Those simulations were done to studied the behaviour of both the charge pump and the UCL. Once that stage was validated through simulation, it was needed to evaluate the impact of adding, firstly, the PV cell as the input voltage source and later the supercapacitor as energy buffer.

The initial test bench can be seen in Figure 4.2. The only change regarding the test bench in Figure 3.12, was replacing the voltage control with the PV cell.

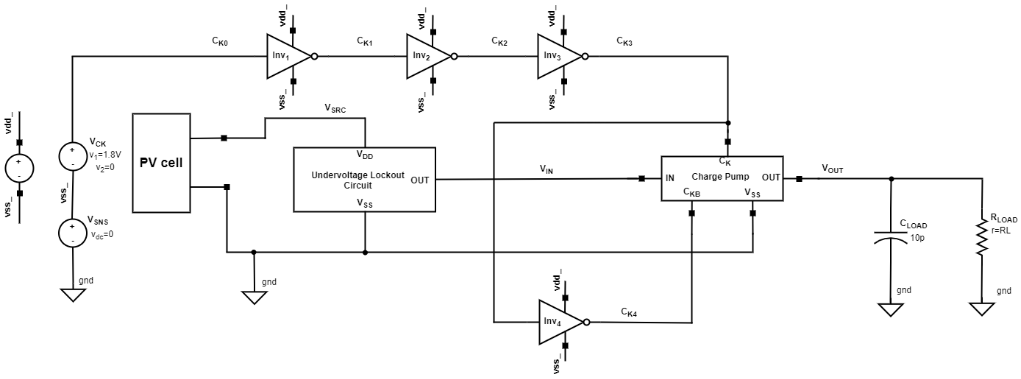

Figure 4.2: Power Conditioning Circuit with PV cell Test Bench

The simulations performed and the parameters studied were the same as in the power conditioning stage. It was once again crucial to get the maximum possible power on the output, achieving a good efficiency ratio. The results can be seen in Figure 4.3.

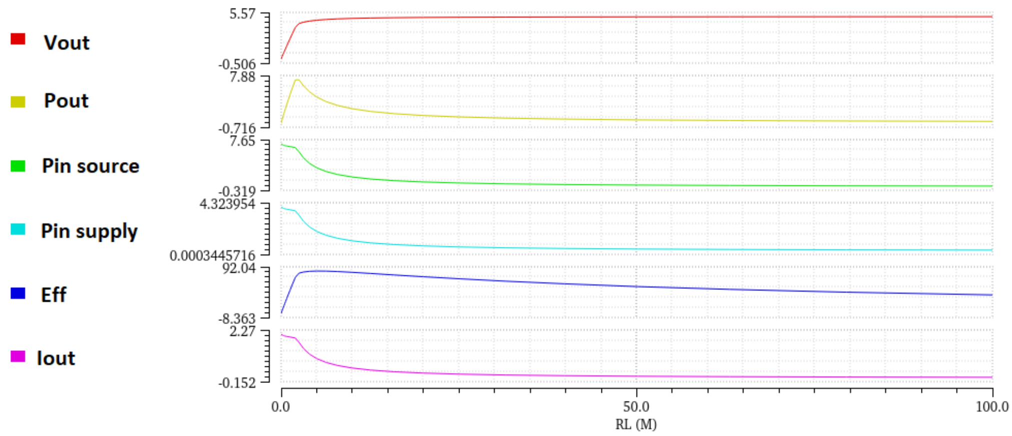

(a)

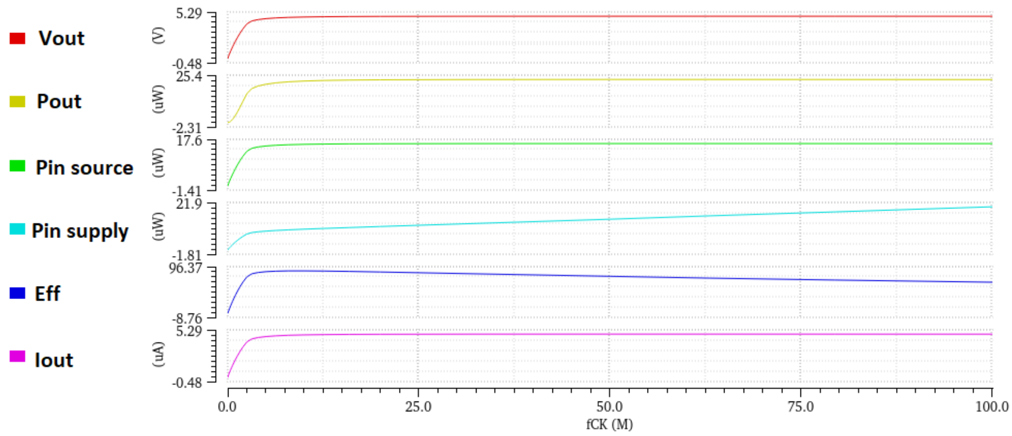

(b)

Figure 4.3: Power Conditioning Circuit with PV cell Analysis (a) with $f_{CK} = 1MHz$ and varying R_{Load} (b) with $R_{Load} = 1M\Omega$ and varying f_{CK}

The behaviour of the system, having the PV cell as the input voltage source, is very close to the performances analysed in the previous chapter. The power stage circuit served its purpose even adding the PV cell. Observing the responses it can be concluded that, once again, increasing the frequency results in an initial increase in the output voltage and therefore an increase in the efficiency, that eventually stabilizes close to the maximum value obtained. When increasing the R_{Load}, P_{OUT} decreases. The efficiency was calculated as in the previous simulations and higher values were attained. With a fixed value of 1MHz for the f_{CK} and varying R_{Load}, the efficiency reached a maximum of 83.67% when $R_{Load} = 5M\Omega$. Fixing R_{Load} at 1MΩ and varying f_{CK}, it was attained a efficiency of 87.6%, the higher value obtained considering all the simulations. Additionally and according to what was done in the previous simulations, a transient analysis was performed, Figure 4.4. Fixing f_{CK} at 5MHz and R_{Load} at 1MΩ it was a achieved an efficiency of 82.68%.

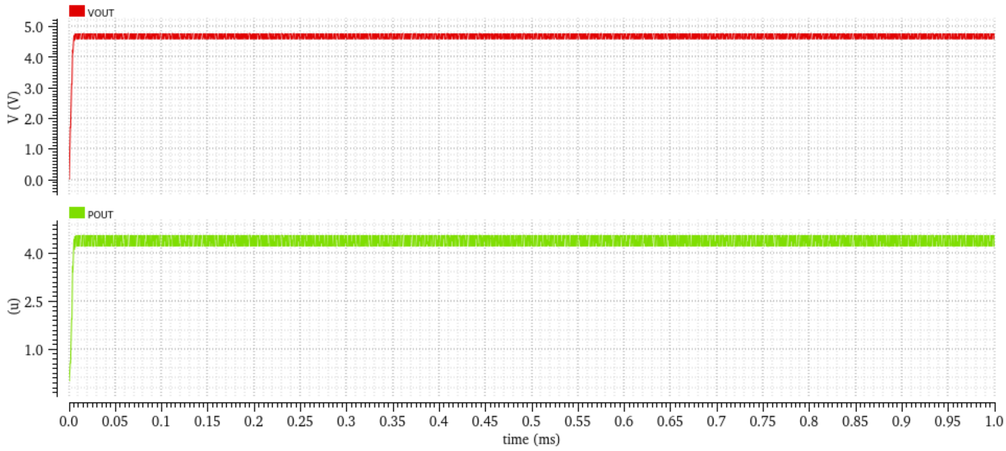

Figure 4.4: Transient Analysis of the PV system

After evaluating the performance of the system with the PV cell as input voltage source, it was in order to studied how the system reacted increasing the capacitance of the load capacitor (C_{Load}), that could become a supercapacitor if it was able to maintain the good performance of the circuit. The test bench used to evaluate the influence of the supercapacitor was the one used in the previous analysis, Figure 4.2. C_{Load} was slowly increased in order to explore how it would affect the PV system. As proceeded in the prior simulations it was performed a PSS analysis.

When increased the C_{Load} to 1uF, significantly higher to the value used in the previous analysis, but not high enough to be considered a supercapacitor, the response was more irregular than prior simulations. The results are shown in Figure 4.5.

The results of this simulation were inconclusive and a transient response was performed in order to comprehend the possible issues with the increased of the C_{Load} value.

There were made several simulations, considering different values for each parameter. All performed poorly regarding the efficiency of the system and failed to reach a steady state for both V_{OUT} and P_{OUT}. One of the responses for the analysis of the PV system with a higher C_{Load} can be seen in Figure 4.6

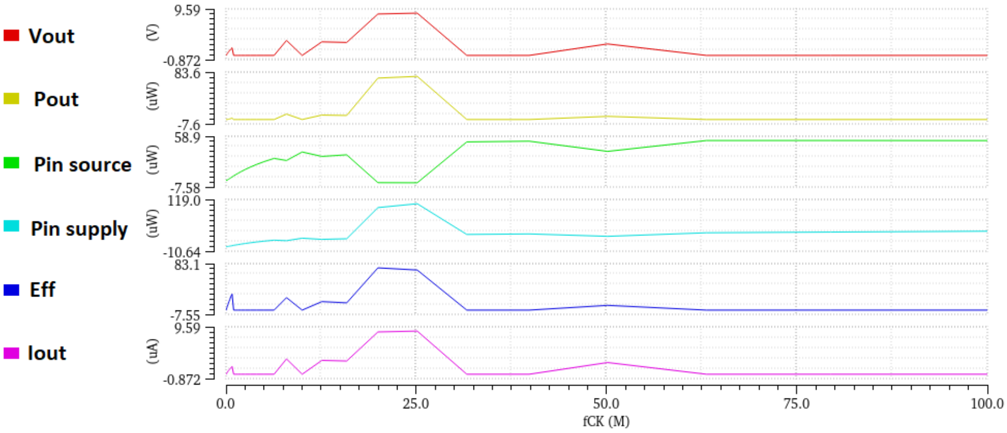

(a)

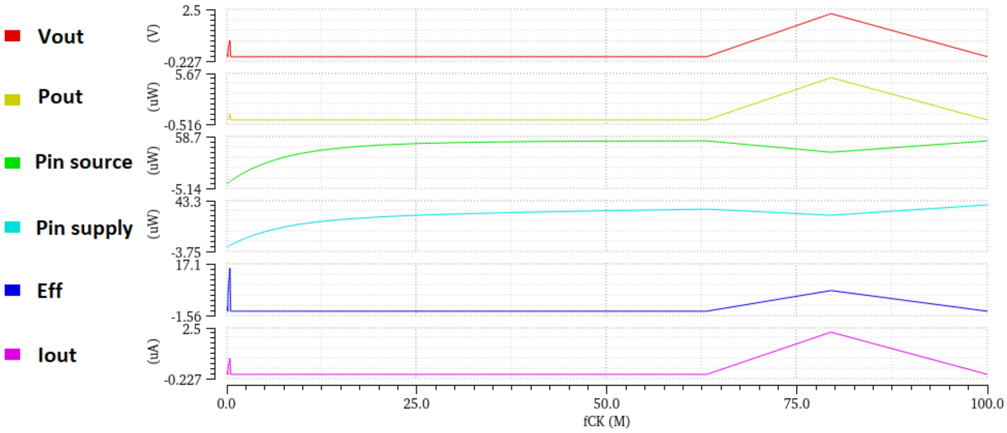

(b)

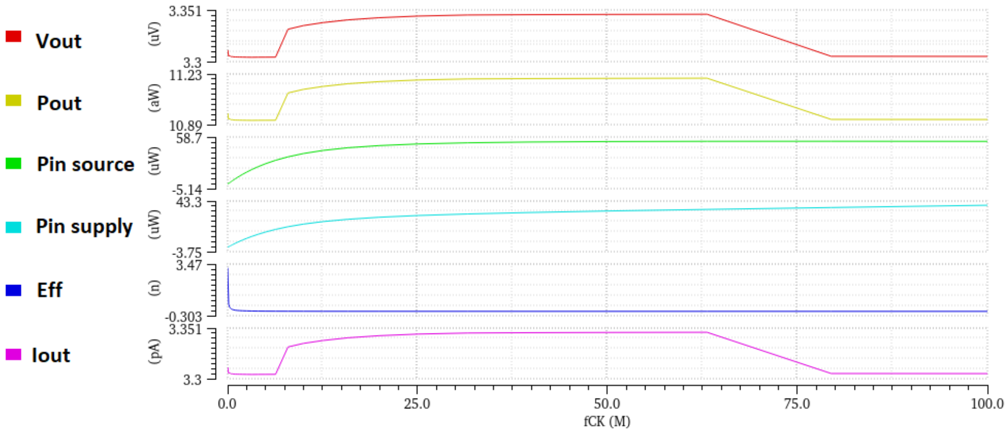

(c)

Figure 4.5: PV system Performance Analysis, varying f_{CK} and $R_{Load} = 1M\Omega$ (a) with $C_{Load} = 1uF$, (b) with $C_{Load} = 100uF$, (c) with $C_{Load} = 10mF$,

This simulation took significantly more time and space that the previous transient analysis and failed to converge. The V_{OUT} did not get the boost relatively to the input voltage as happened in the previous simulations. Thus, P_{OUT} could not reach the high values attained before, resulting in

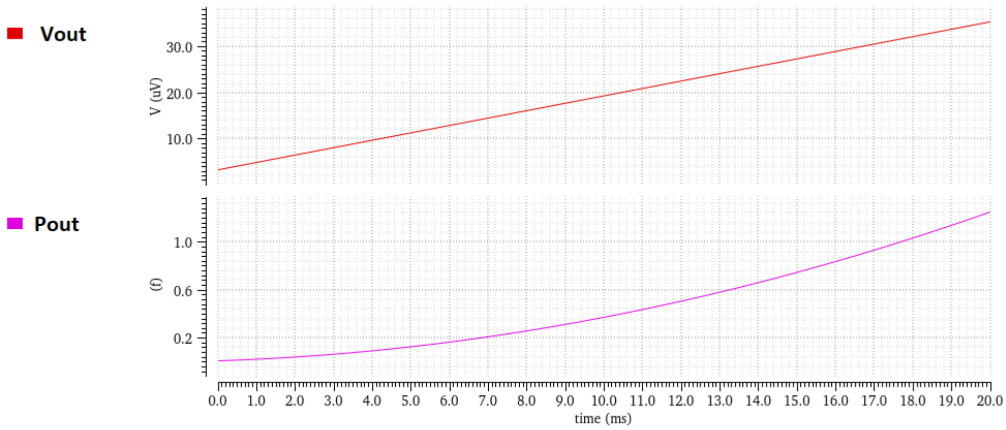

Figure 4.6: Transient Analysis of the PV system with $C_{Load} = 10mF$

a poor efficiency. Therefore the approach for the supercapacitor in the PV system modeled did not performed as expected and proved not to be suitable for this system.

Chapter 5

Conclusions and Future Work

Photovoltaic energy harvesting systems are becoming more relevant for the planet everyday. As the natural resources available to be used by humans to produce energy decrease, relying on either natural sun light or artificial light has proved to have a crucial benefit. Thus, it is expected that this sort of system become more popular with time.

The main contribution of this thesis relies on the Power Conditioning Stage of the presented system. The charge pump topology chosen has proved to be suitable for this type of system, being able to boost the input voltage, the main target of the converter. The Undervoltage Lockout Circuit served its purpose, preventing the system functioning when the voltage available was under the minimum for its correct operation. The two devices combined were able to perform accurately, giving good efficiency results.

The model of the PV cell chosen was appropriate to prove the efficiency of the circuit as a photovoltaic energy harvesting system considering it was possible to attain higher values of efficiency once the PV cell was added to the system.

Regarding the energy storage stage of the system, the results were below expectations. Adding the supercapacitor to the system had a serious and negative impact on the overall performance, as it resulted in a poor V_{OUT} and P_{OUT} performance, which had a direct influence on the efficiency. The approach chosen was not suitable for the PV system aimed to implement.

5.1 Future Work

To conclude this dissertation it is presented future work that could be explored in order to advance in the studies of photovoltaic energy harvesting systems for indoor environments.

- **Implementing a Supercapacitor Array**: Using a single large supercapacitor as energy storage element might seem a simpler approach but can not be adequate for the system, and it is more likely that the harvesting would suffer with two problems:

- **Cold booting**: As explained in Chapter 3, the system is constantly rebooting when there is no energy to operate properly. This phenomenon usually happens when the supercapacitor has a large capacitance which implies the need of more energy to achieve the threshold voltage when compared to a supercapacitor with a smaller capacitance.
- **Inrush Current**: It is a short circuit when the supercapacitor that is working as a load is nearly empty.

Considering the mentioned problems, the best option would be to use a supercapacitor array, composed of more than one supercapacitor and thus solving any issue that could come up with the use of a single large supercapacitor. An example of a supercapacitor that could be implemented is shown in Figure 5.1 (a). It consists of three supercapacitors, the first one with a lower capacitance, which will allow the system to start working even with low energy levels, preventing a cold booting situation. In Figure 5.1 (b) is shown the state machine representing the behaviour of the supercapacitor array.

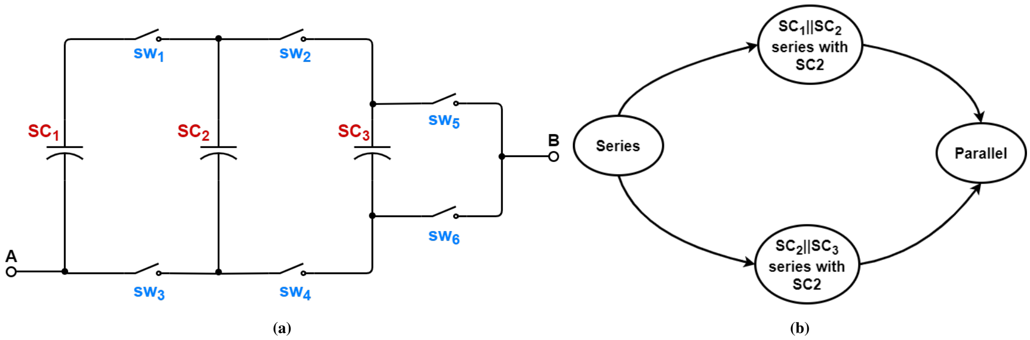

Figure 5.1: (a) Possible Implementation of Supercapacitor Array, (b) Supercapacitor Array State Machine

The array would be controlled by switches, that would be enabled and disabled as desirable. The set of switched array connections is represented on table 5.1.

Table 5.1: Set of switch array connections

	sw1	sw2	sw3	sw4	sw5	sw6
Serie	1	0	0	1	1	0
SC1IISC2	1	1	1	0	0	1
Parallel	1	1	1	1	1	0
SC2IISC3	1	1	0	1	0	1

- **Replacing ideal current sources**: In the test bench used for the ULC it is used an ideal current source that in future experiments could be replaced with a non-ideal version.

- **Evaluate different PV cell models**: In this work, only one PV cell model was tested, it would be interesting as future work to explore the performance of different model and kinds of PV cell and studied the effects on the overall PV system.

Appendix A

```
‘include "constants.vams"
 ‘include "disciplines.vams"
module mypvcell(P1, P2);
inout P1;
electrical P1;
inout P2;
electrical P2;
parameter real ISC=500e-6;
parameter real VOC=3.3;
parameter real h=0.05;
parameter real k=100;
real ipv;
real tmp1;
real tmp2;
analog begin
tmp1 = V(P1,P2)/VOC;
tmp2 = 1-pow(tmp1,k);
ipv = ISC*tmp2/(1+h*(V(P1,P2)/VOC));
I(P2,P1) <+ ipv;
end
endmodule
```

References

[1] RD Prabha and GA Rincón-Mora. CMOS Photovoltaic-Cell Layout Configurations for Harvesting Microsystems. In *2013 IEEE 56th International Midwest Symposium on Circuits and Systems*, pages 368–371. IEEE, 2013.

[2] C Carvalho and N Paulino. CMOS Indoor Light Energy Harvesting System for Wireless Sensing Applications: An Overview. In *Doctoral Conference on Computing, Electrical and Industrial Systems*, volume 470. Springer, 2016.

[3] H Ono, N Nakano, and K Nomura. A Design of CMOS On-Chip Photovoltaic Device and Regulated DC-DC Converter for Micro System. In *Proceedings SASIMI*, pages 25–27, 2013.

[4] M Ferri, D Pinna, E Dallago, and P Malcovati. Integrated Micro-Solar Cell Structures for Harvesting Supplied Microsystems in 0.35-μm CMOS Technology. In *SENSORS*, pages 542–545. IEEE, 2009.

[5] H Shao, CY Tsui, and WH Ki. The Design of a Micro Power Management System for Applications Using Photovoltaic Cells with the Maximum Output Power Control. *IEEE Transactions on Very Large Scale Integration (VLSI) Systems*, 17(8):1138–1142, 2009.

[6] U Çilingiroğlu, B Tar, and Çağatay Ö. On-Chip Photovoltaic Energy Conversion in Bulk-CMOS for Indoor Applications. *IEEE Transactions on Circuits and Systems I: Regular Papers*, 61(8):2491–2504, 2014.

[7] D Batista, LB Oliveira, N Paulino, C Carvalho, J P Oliveira, J Farinhas, A Charas, and journal=Sensors year=2019 volume=19 number=8 pages=1803 publisher=Multidisciplinary Digital Publishing Institute Dos Santos, PM. Combined Organic Photovoltaic Cells and Ultra Low Power CMOS Circuit for Indoor Light Energy Harvesting.

[8] AS Sedra and KC Smith. Microelectronic Circuits. London, 2006.

[9] MG Villalva, JR Gazoli, and E Ruppert Filho. Comprehensive Approach to Modeling and Simulation of Photovoltaic Arrays. *IEEE Transactions on Power Electronics*, 24(5):1198–1208, 2009.

[10] RW Miles, KM Hynes, and I Forbes. Photovoltaic Solar Cells: An Overview of State-of-The-Art Cell Development and Environmental Issues. *Progress in Crystal Growth and Characterization of Materials*, 51(1-3):1–42, 2005.

[11] JF Dickson. On-Chip High-Voltage Generation in MNOS Integrated Circuits Using an Improved Voltage Multiplier Technique. *IEEE Journal of Solid-State Circuits*, 11(3):374–378, 1976.

[12] I Chowdhury. Efficient Voltage Regulation Using Switched Capacitor DC/DC Converter from Battery and Energy Harvesting Power Sources. 2010.

[13] Gaetano Palumbo and Domenico Pappalardo. Charge Pump Circuits: An Overview on Design Strategies and Topologies. *IEEE Circuits and Systems Magazine*, 10(1):31–45, 2010.

[14] Y Allasasmeh and S Gregori. A Performance Comparison of Dickson and Fibonacci Charge Pumps. In *2009 European Conference on Circuit Theory and Design*, pages 599–602. IEEE, 2009.

[15] YH Chang and SY Kuo. High-Gain Serial-Parallel Switched-Capacitor Step-Up DC-DC Converter. In *Proceeding of the International MultiConference of Engineers and Computer Scientists, II*, volume 6, 2012.

[16] JK Kim and GW Moon. Derivation, Analysis, and Comparison of Nonisolated Single-Switch High Step-Up Converters with Low Voltage Stress. *IEEE Transactions on Power Electronics*, 30(3):1336–1344, 2014.

[17] Z Kamal, Q Hassan, and Z Mouhcine. Full on Chip Capacitance PMOS Low Dropout Voltage Regulator. In *2011 International Conference on Multimedia Computing and Systems*, pages 1–4. IEEE, 2011.

[18] I Enne, M Nikolić, and H Zimmermann. Dynamic Integrated MPP Tracker in 0.35 μm CMOS. *IEEE Transactions on Power Electronics*, 28(6):2886–2894, 2012.

[19] RM Sabarillo and CO Mocorro. Indoor Light Energy Harvesting System for Battery Recharging and Wireless Sensor Networks Implemented in 90nm CMOS Technology. In *2015 International Conference on Humanoid, Nanotechnology, Information Technology, Communication and Control, Environment and Management*, pages 1–5. IEEE, 2015.

[20] S Sudevalayam and P Kulkarni. Energy Harvesting Sensor Nodes: Survey and Implications. *IEEE Communications Surveys & Tutorials*, 13(3):443–461, 2010.

[21] J Li, E Murphy, J Winnick, and PA Kohl. The Effects of Pulse Charging on Cycling Characteristics of Commercial Lithium-Ion Batteries. *Journal of Power Sources*, 102(1-2):302–309, 2001.

[22] Y Kim, N Chang, Y Wang, and M Pedram. Maximum Power Transfer Tracking for a Photovoltaic-Supercapacitor Energy System. In *Proceedings of the 16th ACM/IEEE International Symposium on Low Power Electronics and Design*, pages 307–312, 2010.

[23] H Yang and Y Zhang. Analysis of Supercapacitor Energy Loss for Power Management in Environmentally Powered Wireless Sensor Nodes. *IEEE Transactions on Power Electronics*, 28(11):5391–5403, 2013.

[24] Hairul Nissah Zainudin and Saad Mekhilef. Comparison Study of Maximum Power Point Tracker Techniques for PV Systems. 2010.

[25] Hua Yu, Hanzhong Wu, Yumei Wen, and Ping Li. Indoor Micro-Light Energy Harvesting System for Low Power Wireless Sensor Node.

[26] G Waltisperger, C Condemine, and S Basrour. Photovoltaic Energy Harvester for Micro-Scale Applications. In *Proceedings of the 8th IEEE International NEWCAS Conference 2010*, pages 177–180. IEEE, 2010.

[27] JCH Phang, DSH Chan, and JR Phillips. Accurate Analytical Method for the Extraction of Solar Cell Model Parameters. *Electronics Letters*, 20(10):406–408, 1984.

[28] Bidyadhar Subudhi and Raseswari Pradhan. Characteristics Evaluation and Parameter Extraction of a Solar Array based on Experimental Analysis. In *2011 IEEE Ninth International Conference on Power Electronics and Drive Systems*, pages 340–344. IEEE, 2011.

[29] B Subudhi and R Pradhan. A comparative Study On Maximum Power Point Tracking Techniques For Photovoltaic Power Systems. *IEEE Transactions on Sustainable Energy*.

[30] S Pindado and J Cubas. Simple Mathematical Approach to Solar Cell/Panel Behavior based on Datasheet Information. *Renewable Energy*, 103:729–738, 2017.